Part One
Hit Finding and Profiling for Protein Kinases: Assay Development and Screening, Libraries

Protein Kinases as Drug Targets. Edited by B. Klebl, G. Müller, and M. Hamacher

ISBN: 978-3-527-31790-5

1
In Vitro Characterization of Small-Molecule Kinase Inhibitors

Doris Hafenbradl, Matthias Baumann, and Lars Neumann

1.1
Introduction

Typically the starting point for an early-stage drug discovery project is the identification of a small-molecule entity that, among other characteristics, has inhibitory activity against a given target kinase. Kinase inhibitors are usually identified in a high-throughput screening (HTS) campaign. The identified "hits" are selected on the basis of their inhibitory potential against the target kinase, the intellectual property situation around the small-molecule inhibitor class, the potential for further chemical optimization, and other criteria. Once the optimization process has started, several parameters have to be considered and continuously monitored. In most drug discovery programs, the optimization of the inhibitory activity of the small molecules against the target kinase represents the center of activities. While this parameter seems to be a straightforward and measurable parameter, there are a variety of possibilities of how an inhibitor might be binding to a protein kinase. Potentially, these different binding modes can cause modifications of the kinetic binding behavior of the compound. For the full assessment of an inhibitor, a detailed analysis of binding modes and kinetic consequences is required.

The optimization of a specific protein kinase inhibitor requires the constant assessment of a wide range of kinases to reduce the risk of possible side effects. It is therefore important to use comparable conditions in each protein kinase assay.

A successful drug candidate also requires a balanced physicochemical profile that determines the pharmacokinetic (PK) behavior of a small-molecule inhibitor in animals. In the past 10 years, a variety of *in vitro* assays have been developed and proven to be useful for the prediction of the PK parameters of an inhibitor.

Here, we describe in detail a selection of *in vitro* assays that are critical for the optimization process of small-molecule kinase inhibitors. For an appropriate start, a thorough optimization of the biochemical kinase assay is needed. In addition, one needs to consider the mode of inhibition and should be prepared for unexpected exceptions from the general rules. Besides the rationalization of the measurement of the biochemical activity and the selectivity that influence the pharmacodynamic behavior of a small-molecule inhibitor, we will give an in-depth overview of options

Protein Kinases as Drug Targets. Edited by B. Klebl, G. Müller, and M. Hamacher

ISBN: 978-3-527-31790-5

for *in vitro* measurement of parameters that determine the pharmacokinetic behavior of small-molecule inhibitors.

1.2 Optimization of a Biochemical Kinase Assay

At the first glance, a biochemical kinase assay seems to be a very straightforward enterprise with only very few parameters that can be modified: the concentration of ATP, substrate, and protein kinase, the composition of the reaction buffer, and the reaction time. Nevertheless, a detailed optimization process is needed and several considerations have to be taken into account. In the following, we will give guidance for the evaluation of each step of the assay optimization and how this information is used to achieve the goal: a biochemical screening assay that yields reliable and reproducible information about the inhibitory activity of a small molecule as one of the most critical parameters throughout an entire drug discovery project. The optimization process for the AGC kinase Rock II is used as an example for describing in detail the considerations and evaluation of the results.

1.2.1 Step 1: Identification of a Substrate and Controlling of the Linearity between Signal and Kinase Concentration

Finding a substrate that is recognized and efficiently phosphorylated by the kinase of interest is the first essential step in developing a biochemical kinase assay. Equally important is the identification of the kinase concentration to start the assay optimization that guarantees a sufficiently high signal and at the same time good linearity between signal and kinase activity.

When the concentration of kinase is low, the concentration changes in ATP, ADP, and phosphorylated substrate are very small after a given reaction time. As a consequence, the associated assay signal is low and inaccurate (Figure 1.1, region of low assay signal). At moderate kinase concentrations, a sufficiently high assay signal can be detected and at the same time linearity between signal and kinase activity is observed. Thus, for example, a doubling of kinase activity is directly translated into the doubling of the assay signal (Figure 1.1, linear region). At high kinase concentrations, the bulk of ATP or substrate transforms into phosphorylated substrate after the given reaction time and the linearity between kinase activity and assay signal is lost (Figure 1.1, nonlinear region). At very high kinase concentration, all ATP or substrate is converted into ADP and phosphorylated substrate and an even higher kinase concentration cannot increase the signal further (Figure 1.1, insensitive region). Thus, as soon as the assay is depleted of either ATP or substrate, the assay is blind to changes in kinase activity. This situation is detrimental for two reasons. First, if the goal is to improve the assay conditions in order to increase the kinase activity, the assay cannot deliver an answer since changes in the kinase activity do not translate into a change in signal. A further increase in kinase activity cannot be

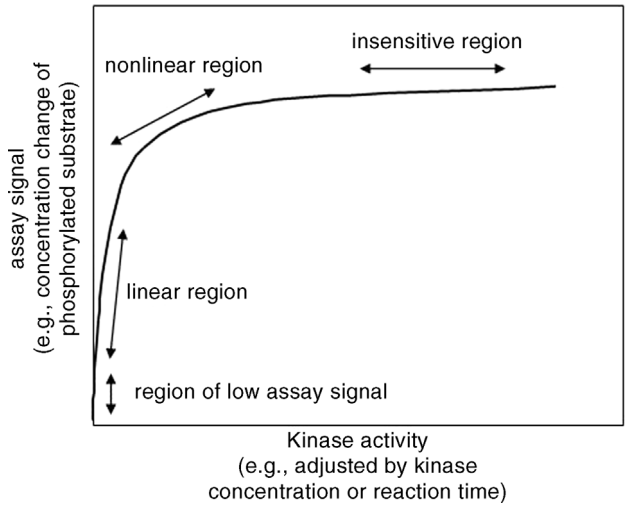

Figure 1.1 Assay signal is plotted against kinase activity. The assay signal can be derived from the concentration change of ATP, ADP, or phosphorylated substrate after the given reaction time. Kinase activity is adjustable, for example, by varying the kinase concentration or reaction time. The plot is separated in four distinct regions. (1) Region of low assay signal at very little kinase activity. In this region, the kinase activity is so low that only very little concentration changes in either educts or product have occurred. Usually, this region yields signals that are too weak to generate reliable data. (2) Linear region. At higher kinase activities, the concentration changes are larger and therefore the assay signals are generally strong enough to give robust data quality. This region is the optimal to perform kinase assays since a change in kinase activity is translated linearly in a signal change. (3) Nonlinear region. At even higher kinase activities, most of the ATP and/or substrate is transformed into ADP and phosphorylated substrate, respectively. In this region, high assay signals can be achieved, but kinase activity and signal do not depend linearly on each other anymore. (4) Insensitive region. If all ATP or substrate is consumed after the investigated reaction time, the maximal possible change of signal has been reached. Increased kinase activity cannot modulate the signal anymore because ATP and/or substrate has been completely consumed. Thus, neither an increase nor a decrease in kinase activity can be detected. In this region, the assay is insensitive to both an improvement of kinase activity (e.g., by optimizing the buffer components) and the inhibition of kinase activity (e.g., by the presence of a kinase inhibitor) and should therefore be avoided implicitly.

detected because even less kinase activity is sufficient to consume all ATP or substrate. Second, in the opposite scenario the question is whether or not a compound reduces the activity of a kinase. If the compound blocks 50% of the kinase activity, no change of the assay signal can be detected, as even 50% kinase activity is sufficient to consume all ATP or substrate within the given reaction time. Therefore, the activity of an inhibitor would be underestimated or the inhibition would not be detected at all.

In the first assay optimization step, both the substrate that yields in the highest kinase activity and the kinase concentration that combines sufficient assay signal and signal linearity are identified. Therefore, a series of potential substrates are tested in

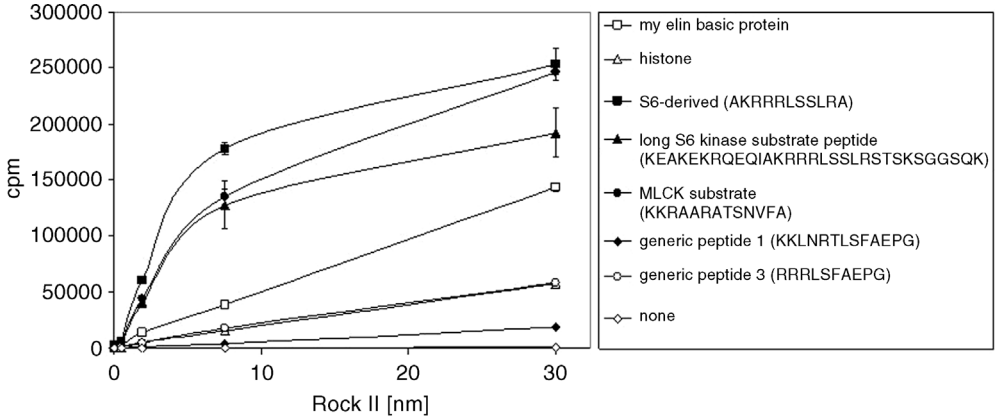

Figure 1.2 10 μM ATP and 12.5 μCi/ml ^{33}P-y-ATP are incubated with increasing concentrations of Rock II and 10 μM of various potential Rock II substrates in 40 μl 20 mM Tris pH 7.5, 10 mM $MgCl_2$, 1 mM DTT for 1 h at room temperature. After 1 h, the reaction was terminated by adding 10 μl 0.5 M EDTA. The reaction mixtures are transferred to phosphor cellulose filters and incubated with 60 μl 0.75% H_3PO_4 for 15 min. Remaining ^{33}P-y-ATP was removed from the filters by three washes with 200 μl 0.75% H_3PO_4 each. The filter-associated substrate-incorporated ^{33}P was quantified by scintillation counting and plotted against Rock II concentration. The error bars are given in standard deviations of duplicates.

the presence of increasing kinase concentrations. In Figure 1.2, step 1 of an assay optimization for the kinase Rock II is exemplified. Seven potential Rock II substrates were incubated with increasing concentrations of Rock II. In addition, Rock II was incubated in the absence of substrate. After 1 h, the reaction was terminated and the amount of phosphorylated substrate quantified. As shown in Figure 1.2, S6-derived peptide is phosphorylated most efficiently yielding the highest assay signal at low kinase concentrations. The generic peptide 3 was recognized with lowest efficiency. In the absence of substrate, consistently no assay signal was detected at all. In the presence of the S6-derived peptide, the linear assay region is found between 0.5 and 7 nM Rock II. Below 0.5 nM Rock II, only very small amounts of S6-derived peptide are phosphorylated and the assay signal is too small to be reliable. At Rock II concentration above 7 nM, the majority of the S6-derived peptide is phosphorylated and the assay reaches its nonlinear region. Thus, from step 1 the following information can be taken into account for the next optimization step: (1) S6-derived peptide is selected to be the substrate that is recognized most efficiently and (2) for the next optimization step, a Rock II concentration of 0.5 nM should be used to guarantee strict linearity between assay signal and kinase activity.

1.2.2 Step 2: Assay Wall and Optimization of the Reaction Buffer

In the second assay optimization step, a reaction buffer is identified that enables the kinase to work at its maximal capacity. In other words, the reaction buffer is

$$IC_{50obs} = IC_{50} + 0.5 \times [kinase]$$

IC_{50}: real IC_{50}
IC_{50obs}: observed IC_{50} at given kinase concentration
[kinase]: kinase concentration

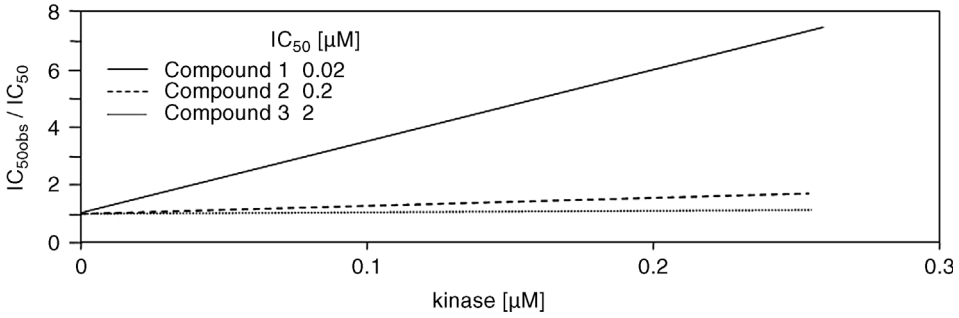

Figure 1.3 The observed IC_{50} (IC_{50obs}) is given by the sum of the real IC_{50} and 0.5-fold the kinase concentration. Consequently, the minimal IC_{50} that can be measured equals 0.5 times the kinase concentration even if the real IC_{50} value is lower. Assays requiring low kinase concentrations – lower than the IC_{50} values of the examined inhibitors – yield IC_{50} values that are very close to the real IC_{50}. The ratio between the observed IC_{50} and the real IC_{50} (IC_{50obs}/IC_{50}) is close to 1. In contrast, assays that need high kinase concentrations – as high as or even higher than the IC_{50} values of the inhibitors – will measure IC_{50obs} larger than the real IC_{50} values. The ratio IC_{50obs}/IC_{50} is above 1 and increases with rising kinase concentrations.

optimized to obtain a sufficiently high assay signal at the lowest possible kinase concentration. Beside the cost considerations, a low kinase concentration is essential since the kinase concentration limits the lowest IC_{50} values that can be determined. The lowest IC_{50} value that can be measured equals half the kinase concentration in the assay (see Figure 1.3) [1, 2]. For example, in an assay that uses 10 nM kinase, the lowest IC_{50} value that can be measured is 5 nM. Even if the real IC_{50} value would be 0.5 nM, the observed IC_{50} revealed by the assay would be 5 nM. This phenomenon is called "assay wall." No IC_{50} value can be measured below this wall defined by the kinase concentration. This behavior is self-evident if one considers that half the kinase molecules have to be bound by an inhibitor to reduce the kinase activity by 50%.

This assay wall can cause a severe impact on drug discovery projects. In the beginning of the project, usually the IC_{50} values are high and far above the kinase concentration. During the course of the project, the IC_{50} values typically decrease with every cycle of compound optimization. At a certain level, the IC_{50} values cannot be decreased anymore. A project course such as this is indicative of having reached the assay wall and it should be constantly monitored if the IC_{50} values have reached the kinase concentration used in the assay.

In the second optimization step, the composition of the reaction buffer is evaluated. The potential addition of detergents, the optimal pH, and ion composition are evaluated to ensure maximal kinase activity. Since kinases are most dependent on Mg^{2+} and Mn^{2+}, these ions should be investigated in great detail. In addition, the

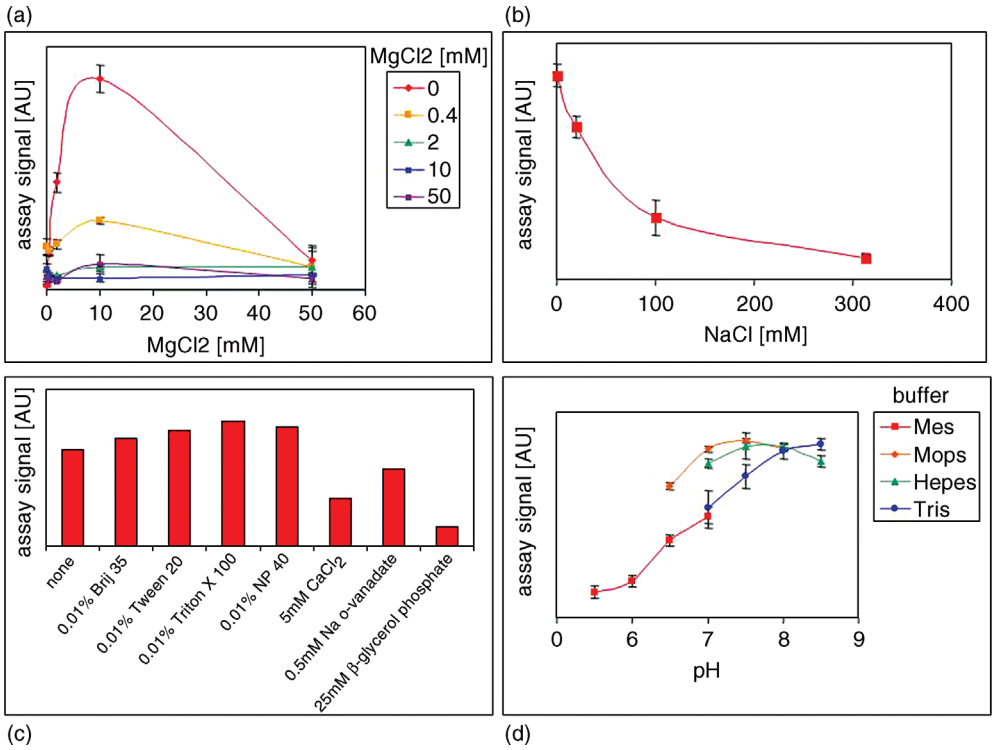

Figure 1.4 1 μM ATP, 12.5 μCi/ml ^{33}P-Y-ATP, 10 μM S6-derived substrate peptide are incubated with 0.5 nM Rock II for 1 h in 40 μl (a) 20 mM Tris pH 7.5, 1 mM DTT, and the indicated amounts of $MgCl_2$ and $MnCl_2$; (b) 20 mM Tris pH 7.5, 10 mM $MgCl_2$, 1 mM DTT, and the indicated concentration of NaCl; (c) 20 mM Tris pH 7.5, 10 mM $MgCl_2$, 1 mM DTT, and the indicated concentrations of detergent, $CaCl_2$, or phosphate inhibitors; or (d) 10 mM $MgCl_2$, 1 mM DTT, and 20 mM of the indicated buffer at the given pH values. After 1 h, the reaction was terminated by adding 10 μl 0.5 M EDTA. The reaction mixtures were transferred to phosphor cellulose filters and incubated with 60 μl 0.75% H_3PO_4 for 15 min. Remaining ^{33}P-Y-ATP, was removed from the filters by three washes with 200 μl 0.75% H_3PO_4 each. The filter-associated substrate-incorporated ^{33}P was quantified by scintillation counting. Error bars are given in standard deviations of duplicates.

influence of NaCl and $CaCl_2$ is examined. Figure 1.4a shows how different combinations of $MgCl_2$ and $MnCl_2$ influence the Rock II activity. A clear maximum in Rock II activity is detected at 10 mM $MgCl_2$ in the absence of $MnCl_2$. Increasing or decreasing the $MgCl_2$ reduces the Rock II activity. Also, addition of $MnCl_2$ results in the loss of Rock II activity. Similarly, the presence of NaCl (Figure 1.4b), $CaCl_2$, and the phosphate inhibitors sodium-*o*-vanadate and β-glycerol phosphate reduces the assay signal (Figure 1.4c). In contrast, the presence of 0.01% detergent such as Brij35, Tween 20, Triton X-100, or NP40 has no significant influence on Rock II performance (Figure 1.4c). Figure 1.4d shows the pH dependence of Rock II. Various buffer systems were used to cover the pH range from 5.5 to 8.5. While Rock II is nearly

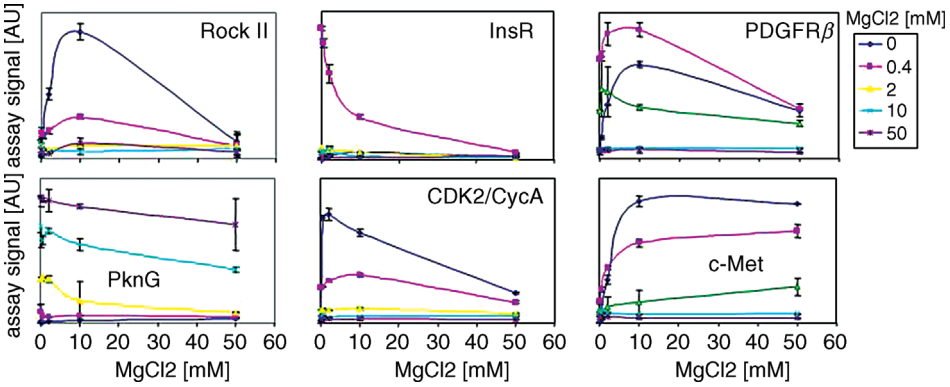

Figure 1.5 Activity of six kinases in the presence of various combinations of $MgCl_2$ and $MnCl_2$ concentrations.

inactive at acidic pH, maximal activity is reached at around pH 7.5. At pH values above 7.5, Rock II loses activity. In summary, on the basis of these results (Figure 1.4), 20 mM Mops pH 7.5, 10 mM $MgCl_2$, 0.01% Triton X-100, 1 mM DTT were chosen as optimal Rock II reaction buffer and were used in the following optimization steps.

The $MgCl_2$/$MnCl_2$ preferences of kinases can widely vary (Figure 1.5). While Rock II prefers 10 mM $MgCl_2$ and the absence of $MnCl_2$, the kinase PknG, for example, is almost inactive under these conditions. PknG shows maximal activity at 50 mM $MnCl_2$ in the absence of $MgCl_2$. On the other hand, PDGFRβ shows highest activity at a combination of 10 mM $MgCl_2$ and 0.4 mM $MnCl_2$. Thus, the optimization of the $MgCl_2$ and $MnCl_2$ concentration for each kinase usually allows to dramatically reduce kinase concentrations in the assay.

In addition to the high diversity in $MgCl_2$/$MnCl_2$ preference, the tolerance for various detergents, $CaCl_2$, and phosphatase inhibitors widely differs between kinases (Figure 1.6), so do pH optima (Figure 1.7). Thus, using a generic kinase reaction buffer for all kinases would result in significantly higher kinase assay concentrations and therefore unnecessarily high assay wall and high assay costs.

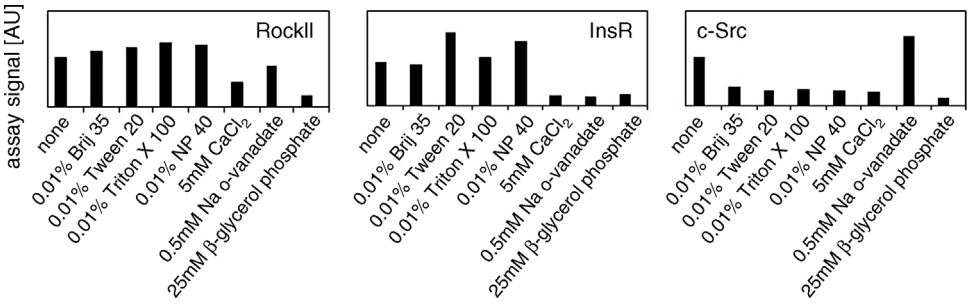

Figure 1.6 Activity of six kinases in the presence of various detergents, ions, and phosphatase inhibitors.

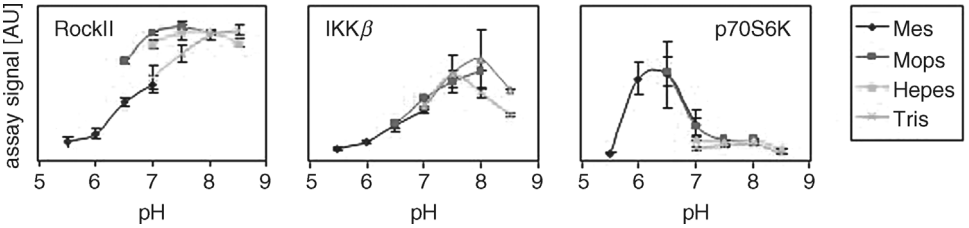

Figure 1.7 Activity of six kinases at various pH values. In order to cover a pH range from 5.5 to 8.5, different buffer systems were used.

1.2.3
Step 3: The Michaelis–Menten Constant K_m and the ATP Concentration

After the identification of a good substrate and the optimal reaction buffer, the next step is the determination of the ATP concentration that should be used. Since the majority of all kinase inhibitors are ATP competitive, the ATP concentration determines the ability of an assay to identify the potential of a given small-molecule kinase inhibitor. Generally, there are three options of choosing the ATP concentration.

The first is to use a standard ATP concentration that is identical in all different protein kinase assays. The main advantage of a standard ATP concentration is the ease of the experimental procedure, especially if a large number of different kinases are regularly screened. The main disadvantage of a kinase assay with a standard ATP concentration, for example, 30 μM or 100 μM, is that the IC_{50} values cannot be used to rank the potency of a given inhibitor between different kinases. For ATP-competitive inhibitors, the dependencies between IC_{50} and ATP concentrations are described by the Cheng–Prusoff equation (Figure 1.8) [3]. The IC_{50} and the ATP concentration are linearly connected. The slope is given by the ratio between the inhibitor constant K_i and the Michaelis–Menten constant for ATP K_m. The y-intercept is defined by the K_i value. The K_i value describes the affinity between inhibitor and kinase, while the K_m value approximates the affinity between ATP and kinase. Since a given inhibitor has different K_i values for every kinase and since every kinase has a different K_m for ATP, slope and y-intercept are different for each kinase. As a consequence, the lines of the Cheng–Prusoff plot intersect each other. Thus, for example, at an arbitrary assay ATP standard concentration of 10 μM, a smaller IC_{50} will be measured for a given inhibitor against a theoretical kinase 1 ($K_{mATP} = 1.5\,\mu M$, $K_i = 0.002\,\mu M$) than against kinase 2 ($K_{mATP} = 10\,\mu M$, $K_i = 0.01\,\mu M$) (Figure 1.8). At an arbitrary ATP standard concentration of 30 μM ATP, the opposite ranking would be observed. At 30 μM, the IC_{50} of the given inhibitor would be measured to be smaller for kinase 2 than for kinase 1 (Figure 1.8). While at one ATP concentration the given inhibitor seems to be more specific for kinase 1, it appears to be more specific for kinase 2 at another ATP concentration. Thus, selectivity ranking based on assays using standard ATP concentrations is arbitrary and therefore should be avoided.

$$IC_{50} = K_I + \frac{K_I}{K_m} \times [ATP]$$

K_m: Michaelis Menten constant
K_i: Inhibitor constant
[ATP]: ATP concentration

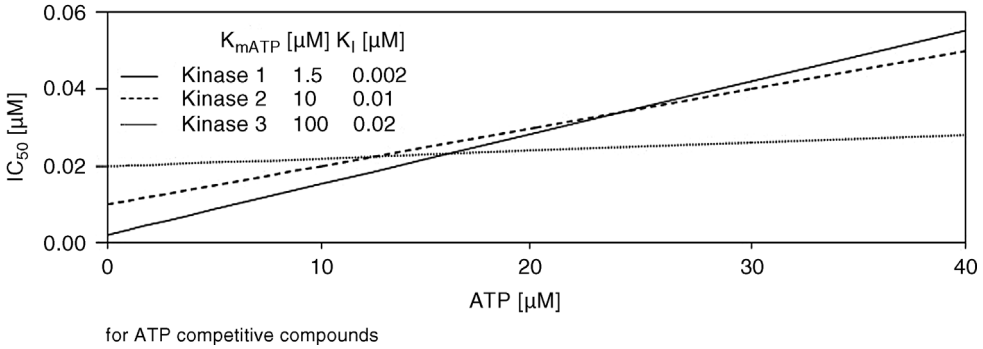

for ATP competitive compounds

Figure 1.8 The Cheng–Prusoff equation describes the dependencies between IC_{50} value and ATP concentration for ATP-competitive inhibitors. The IC_{50} values for one inhibitor against three kinases are calculated for an ATP concentration range from 0 to 40 µM. All three kinases have different K_m values and the K_i values describing the interaction between the theoretical inhibitor and the three kinases vary from 0.002 to 0.02 µM. At ATP concentrations below 12 µM, kinase 1 has the lowest IC_{50} and kinase 3 has the highest IC_{50}. At ATP concentrations between 12 and 17 µM, kinase 2 has the highest and kinase 1 the lowest IC_{50}. Between 17 and 24 µM, kinase 3 has the lowest IC_{50}. Above 24 µM, the IC_{50} ranking is completely the opposite compared to the IC_{50} ranking at ATP concentrations below 12 µM. Thus, the selectivity ranking of the theoretical inhibitor depends on the selected ATP concentration.

The second option is to choose an ATP concentration at the cellular ATP level that is seen by the kinase of interest in the pathologic situation. This approach requires exact knowledge of the ATP concentration in the relevant cellular location within the patient. Unfortunately, little is known about the exact cellular ATP concentrations. Even less is known about fluctuations of ATP concentrations between different locations within a cell, between cells in different tissues, between cancer and noncancer cells, between cells in different stages of their development, and so on. As a consequence, the ATP concentration that would be assumed to mimic the cellular ATP concentration *in vivo* does most likely not reflect the reality. The chosen ATP concentration is more likely to represent another form of an arbitrary ATP standard concentration with the associated problem discussed in the beginning of this section.

The third option for choosing the ATP concentration to measure IC_{50} values for ATP-competitive inhibitors is to use ATP at a concentration that equals its K_m value for the individual kinase. The K_m value is defined by the ATP concentration that allows half maximal reaction velocity. Thus, the ATP concentration would be different for every kinase assay. In addition, the determination of the K_m value for every kinase

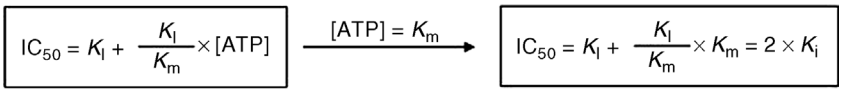

K_m: Michaelis Menten constant
K_i: Inhibitor constant
[ATP]: ATP concentration

Figure 1.9 The Cheng–Prusoff equation describes the relation between IC_{50} value and ATP concentration for ATP-competitive inhibitors. If the ATP concentration equals the K_m value for ATP, the IC_{50} represents twice the K_i value.

is required during the assay development, thereby complicating the assay development and screening workflow. On the other hand, IC_{50} values determined at an ATP concentration that represents its K_m value reflect $2 \times K_i$ value (Figure 1.9). Thus, the IC_{50} value is a direct measure of affinity between the inhibitor and the investigated kinase. As a consequence, the selectivity of an inhibitor against various kinases can be ranked on the basis of its binding affinity for different kinases.

Comparing the three options of choosing an ATP concentration, the K_m value for ATP represents the most advantageous choice when more than one kinase are tested. Since this situation will be found in the majority of all discovery projects, the K_m determination has to be included as the essential step in the assay development. Since the K_m value is defined by the ATP concentration that allows half maximal reaction velocity, the assay signal in the presence of increasing ATP concentrations is measured and fitted to the Michaelis–Menten equation (Figure 1.10) [4]. The ATP K_m for Rock II was determined to be 25 μM. In further assay optimization, 25 μM ATP will be used.

Determination of the ATP K_m of kinases is complicated by the fact that kinases have two substrates, ATP (the phosphate donor) and what we have called the substrate (the phosphate acceptor) so far. Therefore, the ATP K_m depends on the phosphate acceptor concentration. Only if the concentration of the phosphate acceptor is at least five times above its own K_m value, the ATP K_m value is independent of the phosphate acceptor concentration and can be determined precisely. At lower phosphate acceptor concentrations instead of the real ATP K_m, an apparent ATP K_m results from an ATP K_m determination experiment. Under these circumstances, the measured ATP K_m is valid only for the given phosphate acceptor (substrate) concentration.

1.2.4
Step 4: Signal Linearity throughout the Reaction Time and Dependence on the Kinase Concentration

After identifying an appropriate substrate, an optimal reaction buffer, and a meaningful ATP concentration, the selection of assay components is now complete. Step 4 of the assay optimization controls signal linearity if the optimized reaction buffer and adjusted ATP concentration have shifted the range of kinase concentration that guarantees signal linearity compared to assay optimization step 1 (Section 1.1.1). The significance of signal linearity was discussed in Section 1.1.1 (Figure 1.1). In addition,

$$v = \frac{V_{max}\,[ATP]}{K_m + [ATP]}$$

v: reaction velocity; here: assay signal per 1 h
V_{max}: maximal reaction velocity
K_m: Michealis Menten constant for ATP
[ATP]: ATP concentration

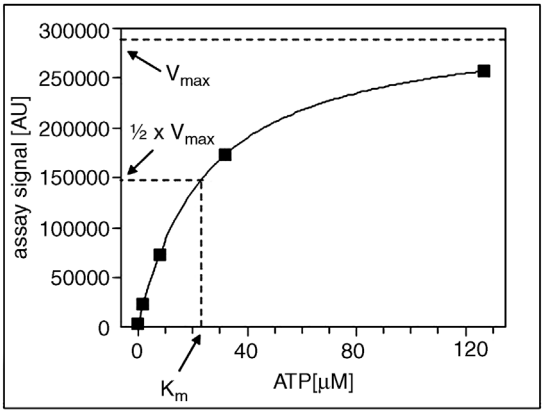

Figure 1.10 The Michaelis–Menten equation describes the dependencies between reaction velocity and ATP concentration. The K_m value is defined by the ATP concentration that results in half maximal reaction velocity. Increasing concentrations of ATP were incubated for 1 h with 0.5 nM Rock II, 2.5 µCi/ml ^{33}P-Y-ATP, and 10 µM S6-derived substrate peptide in 40 µl 20 mM Mops pH 7.5, 10 mM $MgCl_2$, 0.01% Triton X-100, 1 mM DTT. The reaction was terminated by adding 10 µl 0.5 M EDTA and transferred to phosphor cellulose filters followed by an incubation with 60 µl 0.75% H_3PO_4 for 15 min. Remaining ^{33}P-Y-ATP was removed from the filters by three washes with 200 µl 0.75% H_3PO_4 each. The filter-associated substrate-incorporated ^{33}P was quantified by scintillation counting. The assay signal was corrected for the dilution of ^{33}P-Y-ATP in nonradioactive ATP and plotted against the ATP concentration. The data were fitted to the given Michaelis–Menten equation, thereby determining the Rock II ATP K_m to be 25 µM.

step 4 examines the dependency between signal linearity and reaction time. Signal linearity has to be maintained regarding both kinase concentration and reaction time to ensure that the measured IC_{50} (IC_{50obs}) reflects the real IC_{50} (Figure 1.11) [5]. The higher the kinase activity is, regardless whether due to a high kinase concentration or due to a long reaction time, the more the substrate is converted (Figure 1.11a). At high substrate conversion, the measured IC_{50} (IC_{50obs}) is significantly larger than the real IC_{50} (Figure 1.11b). Thus, in order to measure meaningful IC_{50} values, it is essential to identify a combination of kinase concentration and reaction time that has a sufficiently high assay signal and minimal substrate conversion.

In order to identify the Rock II concentration and the Rock II reaction time that guarantees signal linearity, five different Rock II concentrations were incubated at six different reaction times (Figure 1.12). From this experiment, the scientist can pick the optimal combination between Rock II concentration and reaction time. If short

$$\frac{IC_{50obs}}{IC_{50}} = \frac{1 - e^{0.5\ \ln\left(1-\frac{X}{100}\right)}}{\frac{X}{100} - 1 - e^{0.5\ \ln\left(1-\frac{X}{100}\right)}}$$

IC_{50obs}: observed IC_{50} at given substrate conversion
IC_{50}: real IC_{50}
X: substrare conversion [%]

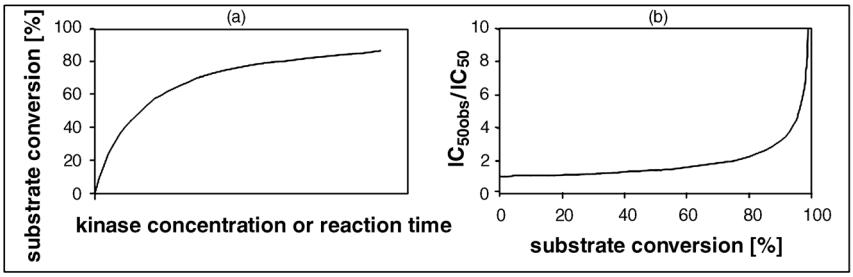

Figure 1.11 The given equation describes the dependency between measured IC_{50} (IC_{50obs}) value and substrate conversion. By increasing kinase concentration at a constant reaction time, or by increasing the reaction time at a constant kinase concentration, more and more substrate will be converted. At very high kinase concentrations or at very long reaction times, 100% of the substrate is converted (a). Using the given equation, the ratio between observed IC_{50obs} and real IC_{50} is plotted against the substrate conversion (b). At substrate conversions above 70%, the observed IC_{50obs} becomes significantly higher than the real IC_{50}.

reaction times are needed, for example, 10 nM Rock II and a reaction time of 60 min can be selected. If low Rock II concentrations are required, for example, to shift the assay wall to lower IC_{50} values (see Section 1.1.2), a Rock II concentration of 2.5 nM and a reaction time of 240 min could be chosen without changing the intensity of the

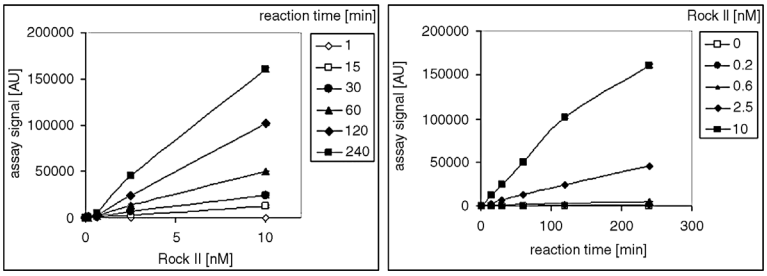

Figure 1.12 Different concentrations of Rock II were incubated for the indicated reaction time with 25 μM ATP, 2.5 μCi/ml ^{33}P-Y-ATP, and 10 μM S6-derived substrate peptide in 40 μl 20 mM Mops pH 7.5, 10 mM $MgCl_2$, 0.01% Triton X-100, 1 mM DTT. Reactions were terminated by adding 10 μl 0.5 M EDTA. The reaction mixtures were transferred to phosphor cellulose filters and incubated with 60 μl 0.75% H_3PO_4 for 15 min. Remaining ^{33}P-Y-ATP was removed from the filters by three washes with 200 μl 0.75% H_3PO_4 each. The filter-associated substrate-incorporated ^{33}P was quantified by scintillation counting. Raw data were plotted either against Rock II concentration (a) or reaction time (b).

assay signal (Figure 1.12). Here, we have chosen 2.5 nM Rock II and a reaction time of 60 min for further optimization.

1.2.5
Step 5: Assay Validation by Measurement of the IC_{50} of Reference Inhibitors

In the last step of the optimization procedure, the assay is validated by the measurement of the IC_{50} values of reference inhibitors. Besides controlling the IC_{50} values themselves, it has to be ensured that the Hill coefficients, reflecting the slope of the IC_{50} curves, are close to a value of 1 (ideally between 0.5 and 1.8). Hill coefficients deviating significantly from 1 indicate that something unexpected is occurring in the assay that in most cases will obscure the measured IC_{50} values. Phenomena such as negative or positive cooperativity of kinase, a contamination with a second kinase that has a different IC_{50} value for the inhibitor from the target kinase, and the presence of different variants of the target kinase (various phosphorylation states, dimers, splice variants, etc.) would influence the Hill coefficient.

In order to validate the optimized Rock II assay, the IC_{50} values of the reference inhibitors H-89 and Y-27632 were measured. The Rock II activity was quantified in increasing concentrations of the reference inhibitors (Figure 1.13). For H-89, an IC_{50} value of 0.18 μM was determined that is in line with the published value of 0.27 μM [6]. The IC_{50} value for Y-27632 was measured to be 0.22 μM. Literature reports a K_i value of 0.14 μM for Y-27632 against Rock II [7]. Since Y-27632 is an ATP-competitive inhibitor and an ATP concentration was used that equals the ATP K_m, the measured IC_{50} value of 0.22 μM translates into a K_i value of 0.11 μM (see Section 1.1.3, Figure 1.9). Thus, the value for Y-27632 was also measured correctly by the developed assay. In addition, the Hill coefficients were calculated to be 1.0 and 0.8, respectively. In conclusion, both the IC_{50} values and the Hill coefficients prove that the optimized Rock II assay is able to measure Rock II IC_{50} values in a reliable manner. Thus, the Rock II assay could be released for a potential Rock II drug discovery project.

1.3
Measuring the Binding Affinity and Residence Time of Unusual Kinase Inhibitors

Besides the classical binding mode, where small-molecule inhibitors bind into the ATP binding cleft forming H-bonds only with the hinge region, there are several known exceptions. Among these kinase inhibitors are examples such as imatinib (**1**), sorafenib (**2**), lapatinib (**3**), and BIRB 796 (**4**, see below).

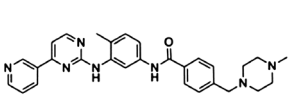

Imatinib (**1**)

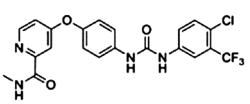

Sorafenib (**2**)

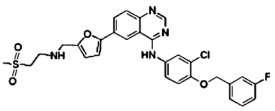

Lapatinib (**3**)

$$\text{activity [\%]} = \frac{100}{1 + \left(\frac{[I]}{IC_{50}}\right)^h}$$

activity: Rock II activity [%]
[I]: inhibitor concentration
IC_{50}: IC_{50} value, inhibitor concentration that yields 50% of Rock II activity
h: Hill coefficient

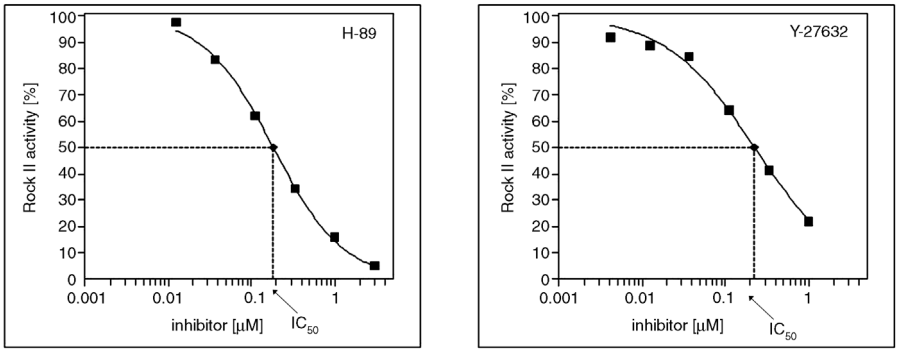

Figure 1.13 2.5 nM Rock II was incubated for 1 h with 25 μM ATP, 2.5 μCi/ml ^{33}P-Y-ATP, and 10 μM S6-derived substrate peptide in 40 μl 20 mM Mops pH 7.5, 10 mM $MgCl_2$, 0.01% Triton X-100, 1 mM DTT in the presence of the indicated concentrations of the reference inhibitor H-89 or Y-27632. Maximal Rock II activity was measured in the absence of inhibitor. Background signal was determined in the absence of Rock II. Reactions were terminated by adding 10 μl 0.5M EDTA. The reaction mixtures were transferred to phosphor cellulose filters and incubated with 60 μl 0.75% H_3PO_4 for 15 min. Remaining ^{33}P-Y-ATP was removed from the filters by three washes with 200 μl 0.75% H_3PO_4 each. The filter-associated substrate-incorporated ^{33}P was quantified by scintillation counting. Rock II activity was expressed by calculating the ratio between the background-corrected assay signals in the absence and presence of the indicated inhibitor concentrations. The Rock II activity was plotted against the inhibitor concentration and fitted to the given equation. For H-89 (a) and Y-27632 (b), IC_{50} values of 0.18 and 0.22 μM and Hill coefficients of 1.0 and 0.8 were calculated, respectively.

These specific inhibitors of protein kinases take advantage of the conformational differences between active and inactive forms of kinases [8]. The main determinant of these forms is the so-called activation loop that can undergo large conformational changes.

Quite often, but not always, these nonclassical inhibitors also show unusual binding characteristics that require special methods for evaluation. The classical way of IC_{50} determination, which has been described in detail in Section 1.1, does not take into account the fact that inhibitors might also show nonclassical enzyme kinetics. Therefore, the activity of these inhibitors might be largely underestimated during the course of an optimization program or might be entirely overlooked in a high-throughput screening campaign.

Several methods have been used in the past to evaluate novel protein kinase inhibitors. To realize the full potential of these nonclassical protein kinase inhibitors,

generic and efficient tools are needed that apply the strengths of diversity-oriented chemical synthesis to the identification and optimization of lead compounds for disease-associated protein kinase targets.

Inactive conformation was first observed crystallographically for the unliganded IR kinase [9], but it was not until the structures of Abl in complex with imatinib and analogues were solved that it became clear that this conformation could be exploited by inhibitors [10] (see also Chapter 6). The so-called DFG-out conformation creates an additional hydrophobic pocket adjacent to the ATP pocket that is frequently referred to as the "allosteric site" [11] or the "deep pocket." Because the amino acids surrounding this pocket are less conserved relative to those in the ATP binding pocket, it has been proposed that it may be easier to achieve kinase selectivity with "deep pocket" binding inhibitors [12] compared to the classical inhibitors.

Very often these nonclassical inhibitors show remarkable cellular activity that could result from binding to the inactive conformation of kinases that may be more accessible in the cellular environment.

It has been discussed that the departure from the kinase–ligand equilibrium interaction comprises an important determinant of the *in vivo* effectiveness of small-molecule drugs. Copeland *et al.* propose that the most crucial factor for sustained drug efficacy *in vivo* is not the apparent affinity of the drug to its target *per se*, but rather the residence time of the drug molecule on its molecular target [13].

The term residence time in the field of drug target interaction is defined as the period for which the receptor is occupied by a ligand. A long dissociation half-life of an intracellular receptor would be expected to translate into sustained efficacy in cell culture after removal of the ligand supply from the extracellular medium. For the *in vivo* situation, the duration of efficacy of a ligand is no longer well described by the *in vitro* measured dissociation constant, but rather depends on the rate of receptor–ligand association (k_{on}) and, most critically, on the dissociation rate constant, or off rate (k_{off}), of the receptor–ligand complex. The off rate can be simply translated into a dissociative half-life for the receptor–ligand complex, and this half-life is a direct measure of the residence time (see Figure 1.14). As demonstrated in a simulation (Figure 1.15), the residence time becomes the driving parameter for the efficacy and the pharmcodynamic behavior of a drug candidate *in vivo*, especially when the plasma half-life is short. Over time, cKIT with *low* binding affinity but *long* compound residence time is more efficiently inhibited than DDR1 with its *high* binding affinity but *short* residence time.

Both the improvement of the metabolic stability and the residence time can be used to optimize the efficacy of an inhibitor compound. As shown in the simulation, the affinity data alone would be a misleading parameter. In addition to the efficacy, the *in vivo* selectivity is affected both by the affinity and by the residence time (Figure 1.15).

Various experimental approaches have been considered to analyze new protein kinase inhibitors. In recent years, the pharmaceutical industry has identified the need both for the discovery of inhibitors with novel modes of inhibition and for the detailed characterization of their lead compounds in preparation for clinical assess-

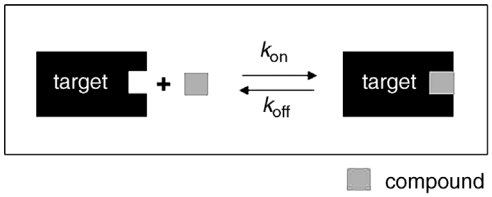

$$\text{residence time} = \frac{1}{k_{off}} \qquad \frac{k_{off}}{k_{on}} = K_d$$

Figure 1.14 Association and dissociation of a receptor–ligand complex and calculations of the parameters residence time, k_{off}, k_{on}, and K_d.

ment. A selection of methods will be discussed and the advantages and disadvantages will be compared.

1.3.1
Washout Experiments

A recent example of the effects of ligand dissociation half-life comes from the work of Wood *et al*. on inhibitors of epidermal growth factor receptor (EGFR) tyrosine kinase activity [14]. The K_d values, off rates, and the recovery of cellular proliferation after washout for three similarly potent inhibitors of EGFR were measured: GW572016 (lapatinib (**3**)), ZD-1839 (Iressa), and OSI-774 (Tarceva). These compounds bind to the ATP binding pocket of the kinase, but display maximum affinity for different conformation states of the enzyme. For ZD-1839 and OSI-774, a rapid recovery of the

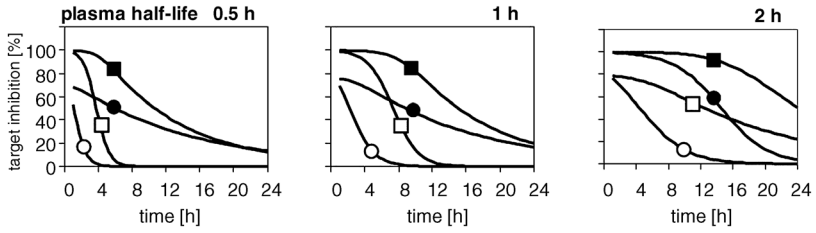

target	k_d [μM]*	residence time [min]	affinity / residence time
■ CDK8-CycC	0.030	576	high / long
● DDR1	0.072	24	high / short
□ cKIT	2.3	811	low / long
○ TAOK3	2.2	1.6	low / short

Figure 1.15 Simulation of *in vivo* inhibition of four targets of the bRaf inhibitor sorafenib: impact of residence time and K_d on pharmacodynamics for three hypothetical compound plasma half-lives ($C_{max} = 10\,\mu M$). Especially for drugs with short or medium plasma half-lives, *in vivo* target inhibition is determined by binding kinetics rather than by binding affinity.

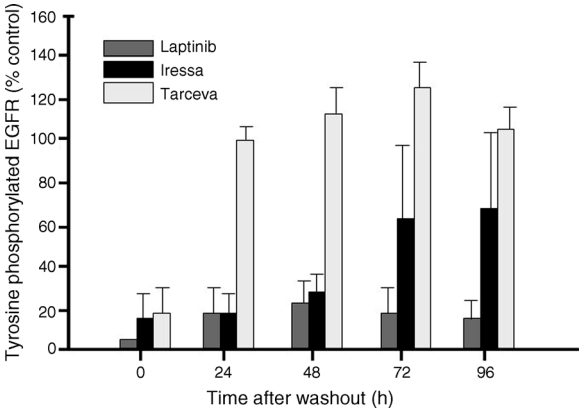

Figure 1.16 Recovery of EGFR autophosphorylation after treatment with lapatinib, Iressa, and Tarceva. Logarithmically growing HN5 cells were treated with 1 μmol/l inhibitor in culture media for 4 h. The media was removed, cells were washed twice, and fresh compound-free media was added. The cells were lysed at the indicated time after inhibitor washout and EGFR was isolated by immunoprecipitation. The level of tyrosine-phosphorylated EGFR was quantified for each condition and expressed as the percentage of vehicle-treated sample. The results represent the mean value of three independent experiments (adapted from Ref. [14]).

kinase activity was observed after washing out the compound. In contrast, the recovery was very slow after treatment with GW572016 (see Figure 1.16).

These data provide a clear example of the extended duration of cellular efficacy that can be achieved with drugs that have long dissociative half-lives. In addition, these data illustrate that the duration of cellular effects of slow dissociating ligands is much longer than would be predicted simply from a consideration of the dissociative half-life of the receptor–ligand complex.

1.3.2
Surface Plasmon Resonance

For the real-time and label-free determination of protein kinase inhibitor binding kinetics, surface plasmon resonance (SPR)-based biomolecular interaction analysis has been used [15, 16].

Specifically for protein kinase, mild immobilization conditions of the kinases to the surface and a carefully composed assay buffer are usually key success factors. With the SPR technology, both direct binding studies of compounds to immobilized kinase and kinase activity assays to confirm inhibitory effects can be performed. Furthermore, detailed kinetic analyses of inhibitor binding and competition assays with ATP for the identification of competitive inhibitors can be determined [16].

The SPR technology requires a sensor surface where typically the protein is immobilized. Using the flow system of the instrument, the analyte passes over the sensor surface. The interaction kinetic, that is, the rates of complex formation (k_a) and

dissociation (k_d), can be determined from the information provided by the sensorgram.

If binding occurs as the sample passes over the prepared sensor surface, the response in the sensorgram increases. If equilibrium is reached, a constant signal will be seen.

Replacing the sample with buffer causes the bound molecules to dissociate and the response decreases. On the basis of the online monitoring of the association and the dissociation process, k_{on}, k_{off}, and K_d can be determined (Figure 1.17).

Among others, p38alpha mitogen-activated protein kinase has been used as a model system. p38alpha MAP kinase has been immobilized to use it as a highly active protein surface, which is the critical and often limiting factor in the development of biosensor methods. In this specific biosensor method, a ligand-induced structural stabilization of p38alpha step was performed during the immobilization step, which should also prove useful for other kinases and ligands [15].

The SPR-based methods can also provide an efficient way to directly and reproducibly examine dissociation constants, kinetics, and even thermodynamics for small-molecule binding with the limitation that one binding partner, typically the protein, has to be bound to the surface of a chip.

Significant progress has been made in recent years in addressing some of the limitations of the SPR technology. Both the throughput and the sensitivity have been dramatically increased. The instruments, including the software, have meanwhile been adapted to a high-throughput use. Rich and Myszka [17] have summarized the most advanced instruments and approaches to higher throughput.

While SPR is the most direct method to evaluate the kinetic behavior of enzymes and inhibitors, the availability of highly pure and homogeneous protein is sometimes

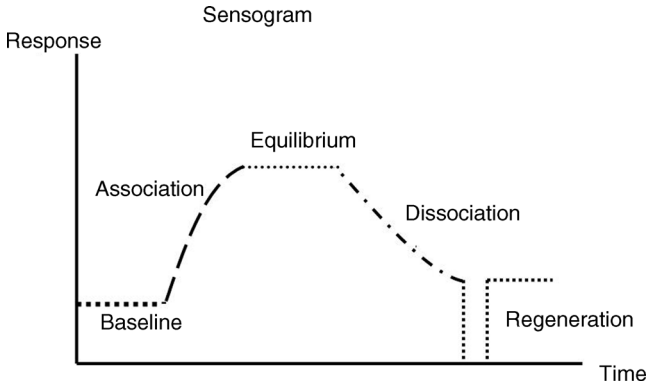

Figure 1.17 Surface plasmon resonance sensorgram. The binding of the analyte to the surface, which is typically coated with protein, is monitored online until the equilibrium is reached. Addition of the buffer causes dissociation of the analyte. When the baseline level is reached, the surface can be regenerated and is used for the next experiment. The concentration- and time-dependent association and dissociation of the analyte allow the calculation of K_d, k_{on}, and k_{off}.

limiting. In addition, the study of full-length proteins and protein complexes is still a challenge.

1.3.3
Classical Methods with Fluorescent Probes

The most widely explored slow inhibitor target interaction is that of BIRB796 with p38alpha [18–20]. The apparent IC_{50} decreases as the time of preincubation with the inhibitor increases.

The interaction of the diaryl urea series that led to BIRB796 has been guided by a fluorescence-based assay, where the kinase in solution was studied with a fluoroprobe. The fluorescence-based assay has been established that is capable of monitoring binding in real time. The binding of the fluoroprobe of a classical inhibitor to nonactivated p38 MAP kinase was quite rapid and required the use of a stopped flow spectrophotometer to determine kinetic rate constants (Table 1.1).

Similarly, the classical ATP site binding inhibitor SB203580 has fast association and dissociation rates for the kinase. In contrast, the association of a fluorescent analogue of BIRB796 with p38MAP kinase is much slower. The calculated half-life for the dissociation of BIRB from p38MAP kinase is 23 h. BIRB796 represents one of the most potent and slowest dissociating inhibitors against human p38 MAP kinase known at present.

Table 1.1 *In vitro* data for selected p38 inhibitors.

	k_{on} ($M^{-1}s^{-1}$)	k_{off} (s^{-1})	K_d (nM)
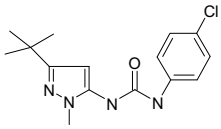	$1.2 \times 10^5 \pm 3\ 5 \times 10^4$	$1.4 \times 10^{-1} \pm 1.2 \times 10^{-2}$	1160
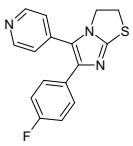	$4.3 \times 10^7 \pm 2.2 \times 10^5$	$7.7 \pm 13 \times 10^{-1}$	180
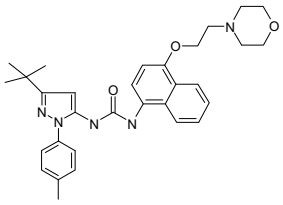	$8.5 \times 10^4 \pm 2.6 \times 10^2$	$8.3 \times 10^{-6} \pm 1.5 \times 10^{-7}$	0.1

K_d was determined at 23 °C and calculated as k_{off}/k_{on} in nM determined with a fluoroprobe assay (see Ref. [18]).

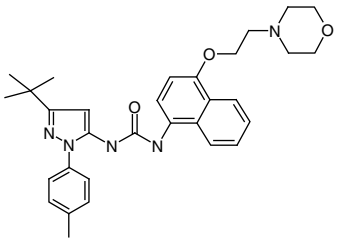

Birb796 (4)

The fluoroprobe assays are very easy to use, but are limited by the availability of a suitable fluoroprobe addressing the binding site of interest.

1.3.4
Preincubation of Target and Inhibitor

To further confirm the slow binding behavior, Kroe *et al*. [18] also monitored the apparent inhibitory potency of BIRB796 as a function of the preincubation time in a standard IC_{50} experiment. A decrease in the apparent IC_{50} value from 97 to 8 nM after 2 h of preincubation is consistent with the slow binding behavior. In contrast, the pyridinyl-imidazole inhibitors reached equilibrium within 30 min.

Another example where preincubation experiments have been valuable for the determination of the kinetic interaction is the inhibitor sorafenib and its interaction with the protein kinase bRaf (Figure 1.18) [21, 22] (Neumann *et al.*, unpublished data). While the activity of the enzyme remains the same, the IC_{50} significantly decreases with increased preincubation.

This type of preincubation experiments can be routinely used to determine very slow binding kinetics using the routine kinase assay as described in Section 1.1. The limitation here is that a kinetic resolution is not possible during the incubation time of the assay. Therefore, these assays are limited to extremely slow compound–target interactions.

1.3.5
Reporter Displacement Assay

A reporter displacement binding assay has been described by Neumann *et al.* [23] that allows to study the kinetic interaction in 384-well format with very little protein requirement, solving the issues of limited throughput and the need for large quantities of protein. The reporter displacement assay is based on a reporter probe that is distinctively designed to bind to the ATP binding site of the protein kinase target. The proximity between reporter and protein results in the emission of an optical signal (Figures 1.19 and 1.20). Compounds that bind to the same binding site displace the probe and cause signal loss. The reporter displacement assay is a homogeneous method that can be used both for the DFG-in and for the DFG-out conformation of the protein kinase. The displacement of the reporter is continuously

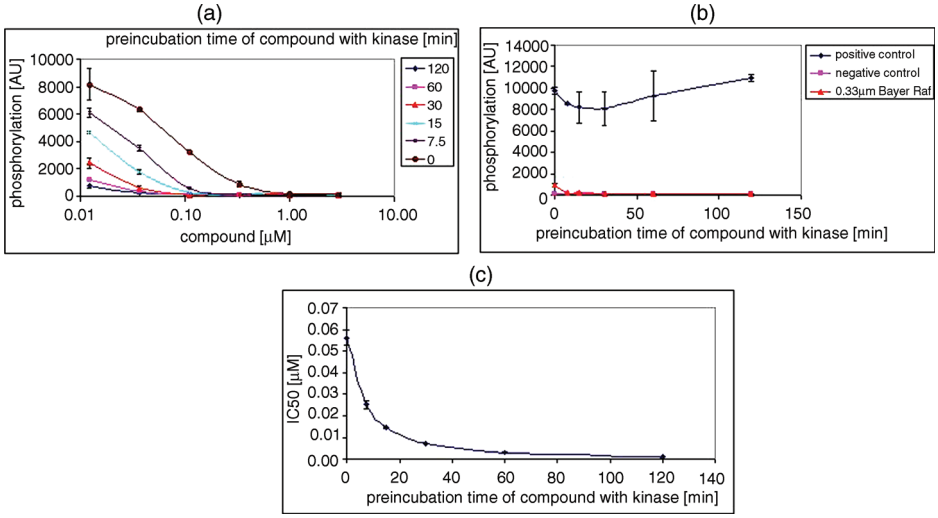

Figure 1.18 Preincubation experiments with sorafenib and bRaf were performed using the radioactive assay as described in Section 1.1. (a) The phosphorylation of the substrate peptide is monitored over a range of compound concentrations and different preincubation times; (b) to monitor the stability and the activity of the bRaf kinase during the incubation period, the phosphorylation of the peptide substrate is monitored in parallel to the increased preincubation time; and (c) the IC_{50} values are calculated for each time point of preincubation, resulting in a significant decrease in IC_{50} over time.

measured over time. The signal for full probe binding is measured in the absence of compound and the signal for complete reporter displacement is quantified in the absence of protein kinase. The reporter probe is designed to have fast association and dissociation kinetics in order to ensure that compound binding and not reporter probe dissociation is the rate-limiting step. The signal decay describes directly the association of the compound with protein kinase. In order to calculate k_{on} and k_{off} of the protein inhibitor interaction signal, the observed association rate k_{obs} is determined for each inhibitor concentration by fitting the corresponding signal decay with a monoexponential decay equation. The exponential coefficient of each monoexponential fit equals k_{obs} for the particular inhibitor concentration. The resulting k_{obs} values were plotted against their inhibitor concentration and fitted to Equation 1.1 describing the dependency between the observed association rate k_{obs}, the association rate k_{on}, the dissociation rate k_{off}, and the inhibitor concentration. The dissociation rate k_{off} is given by the y-intercept and the association rate k_{on} by the slope of dependency between k_{obs} and [inhibitor]. Residence time is calculated by Equation 1.2.

$$k_{obs} = k_{off} + k_{on}[\text{inhibitor}] \tag{1.1}$$

$$\text{Residence time} = 1/k_{off} \tag{1.2}$$

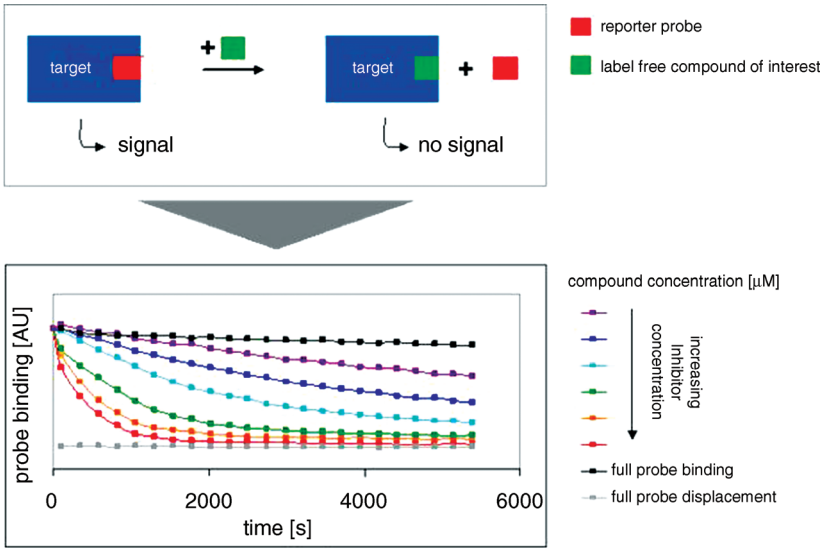

Figure 1.19 Assay principle of the reporter displacement binding assay. Binding of the reporter probe generates a specific signal. Displacement of the reporter probe by a competing compound of interest results in signal loss. By analyzing the kinetics of signal loss at various compound concentrations, values such as K_d, k_{on}, k_{off}, and residence time can be calculated.

The reporter displacement binding assay allows the testing of entire compound series, compound collections, and specifically designed compounds and requires extremely low protein concentrations. The technology is limited by the design of a proper reporter probe addressing the binding site of the kinase of interest.

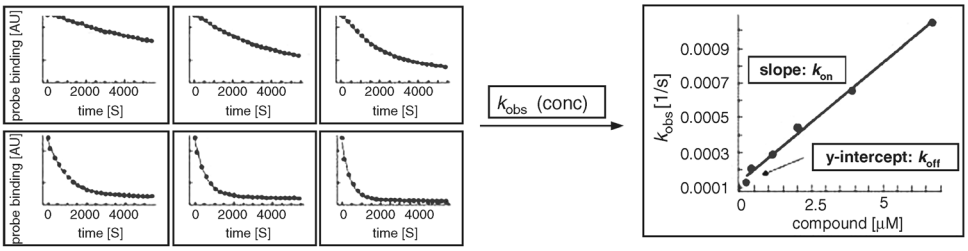

Figure 1.20 Exponential coefficient k_{obs} for each inhibitor concentration is calculated by fitting the signal decays with a monoexponential decay equation. The k_{obs} values were plotted against the corresponding inhibitor concentration and k_{on} and k_{off} were determined by fitting to Equation 1.1. For the plot, only k_{obs} values are used that are well defined. Those k_{obs} values were omitted from analysis if signal decay for a particular inhibitor concentration was faster than the detection limit of the reporter displacement assay or if no significant reporter displacement occurred at low inhibitor concentration.

1.3.6
Implications for Drug Discovery

The lack of high-throughput technologies for measuring the residence time throughout a lead finding and optimization program has limited the number of programs where the residence time has actually been used in parallel to affinity data in the past. The increased availability of such data is inspiring the medicinal and computational chemists to design and synthesize novel compounds. Many different design principles specifically geared toward compounds with long residence times have recently been published [23–25a,b].

Besides the specific synthesis of slow interaction inhibitors, there is also need for the measurement of interaction kinetics if short residence times are required. Nonclassical inhibitors need special consideration both in the hit identification process and in the lead optimization phase. There are a number of challenges in the identification and characterization of compounds that prevent the activation of protein kinases or induce conformational changes. Understanding the relationship between compound structure and biological activity is key to drug design. The mechanism of active compounds must be deconvoluted to determine their functionality. Binding studies are often used for the kinetic analysis of inhibitors, but enzyme activity assays are equally important since only the inhibition of the enzymatic activity will typically lead to a cellular active inhibitor.

With more and more slower interaction inhibitors being characterized in detail, there are new questions arising in the field. It is not known which kinases are amendable to the so-called "deep pocket" binding inhibitors. *In silico* predictions are ongoing to determine the status of such binding capacities [26] and programs are specifically designed for their predictions. The number of deep pocket binders is still too limited to answer the question if the inhibitor is inducing the DFG-out binding or if the kinase is available for this type of binding. In addition, the selectivity profiles of most of the deep pocket binding inhibitors have been determined only in one dimension: the K_d values are available for a vast number of kinases. The question is can these K_d values be trusted, considering that preincubation with the inhibitor might significantly change the K_d value. Neumann *et al.* (submitted for publication) have determined for the first time the kinetic selectivity panel of the bRaf inhibitor sorafenib. The residence times for one inhibitor against a set of protein kinases ranges from a few seconds to 300 min significantly influencing the impact on the pharmacodynamic behavior of such a compound.

The residence time plays a major role especially in the case when the metabolic stability of the inhibitor is very short. Long residence time on the target can help introduce a better *in vivo* selectivity of an inhibitor and can help overcome the pharmacological shortcomings of an inhibitor. The challenges concerning the pharmacology of protein kinase inhibitors will be discussed in Section 1.4.

1.4
Addressing ADME Issues of Protein Kinase Inhibitors in Early Drug Discovery

1.4.1
Introduction

Ideally, the optimization process of potential hits to leads and finally to candidates suitable for preclinical and clinical trials should be guided not only by good pharmacodynamic (PD) parameters but also by satisfactory pharmacokinetic parameters in order to avoid attrition during drug development [27]. The PK behavior of an administered drug is determined by processes such as absorption, distribution, metabolism, and excretion (commonly referred to as ADME processes). Mainly during the past two decades, a toolbox of diverse *in vitro* ADME technologies has been elaborated that enables scientists to filter promising drug candidates at an early stage of drug discovery when usually only few *in vivo* data are available [28, 29].

According to the Traxler's pharmacophore model of small-molecule compounds binding to the active site of protein kinases, ATP-competitive protein kinase inhibitors need to incorporate certain structural and physicochemical specificity determinants to be able to fit into the catalytic cleft of the target protein kinase in an appropriate manner (Figure 1.21). Due to the conservation of structural features within the ATP binding cleft, the physicochemical requirements are quite similar across different classes of protein kinase compounds.

However, as much as the required determinants are crucial for the potency and selectivity of small-molecule compounds, they might translate into poor ADME/PK parameters. This especially holds true for ATP-competitive protein kinase inhibitors as they usually carry lipophilic functional groups that extend more or less deeply into

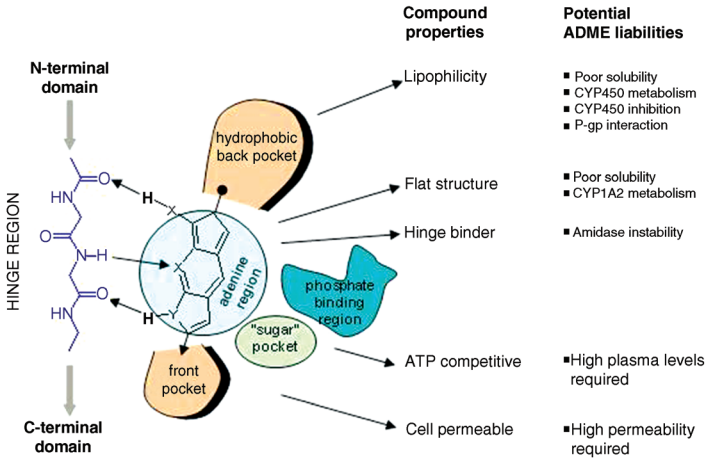

Figure 1.21 Potential ADME issues of small-molecule inhibitors binding to the catalytic cleft of protein kinases according to Traxler's pharmacophore model.

the hydrophobic backpocket of the target kinase. Common ADME liabilities associated with lipophilic moieties are poor solubility, enhanced metabolism by or inhibition of cytochrome P450 enzymes (CYP450s), and the interaction with transporter proteins such as P-glycoprotein (P-gp). Moreover, ATP-competitive protein kinase inhibitors have to efficiently penetrate cellular membranes in order to bind their target. As a consequence, both high plasma levels and high cell membrane permeability are mandatory to reach intracellular compound concentrations high enough to compete with intracellular ATP levels (Figure 1.21).

Thus, expected PK liabilities of ATP-competitive protein kinase inhibitors are likely to deal with insufficient drug absorption and increased drug metabolism raising the need for an ADME screening platform specifically adapted to protein kinase drug discovery programs. The implementation of such a kinase inhibitor-directed ADME approach should be beneficial to identify potential PK problems early in the discovery process and help circumvent these problems in parallel to the optimization of potency and selectivity of kinase inhibitor compounds.

This section will give a brief overview of *in vitro* technologies that address ADME-related characteristics of ATP-competitive protein kinase inhibitors that are most relevant for the routine screening of compounds in the drug discovery phase (Table 1.2). It will mainly focus on the context and the methodologies addressing drug absorption and drug metabolism as the two most crucial *in vitro* PK parameters for protein kinase inhibitors.

Table 1.2 Overview of *in vitro* assays relevant to address potential ADME liabilities of ATP-competitive protein kinase inhibitors in the drug discovery phase.

PK parameter	Assay	Method	Reference
Absorption	Solubility	Shake flask (solution in equilibrium)	[64]
		Turbidimetry	[33]
		Nephelometry	[65]
		Direct UV spectroscopy	[66]
Absorption/volume of distribution	Lipophilicity	Shake flask (partition in octanol versus water/buffer)	[67]
		Direct chromatography	[68]
Absorption	Ionization (pK_a)	pH-metric titration	[69]
Absorption/oral bioavailability	Permeability	PAMPA	[38]
		Caco-2	[41]
Absorption/excretion/ CNS penetration	P-gp interaction	Monolayer efflux	[45]
		ATPase	[70]
		Calcein AM	
Metabolism	Hepatocyte stability	Intrinsic clearance	[57]
	Microsomal stability		[58]
Drug–drug interaction	CYP450 inhibition	Fluorescence-based IC_{50}/ K_i determination	[61]

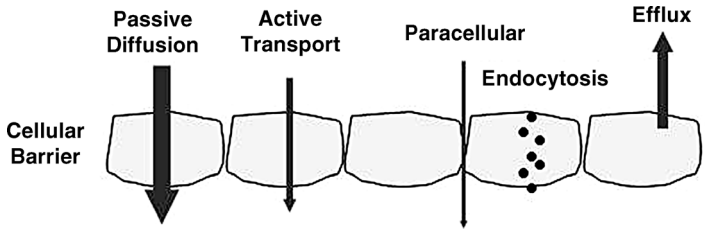

Figure 1.22 Mechanisms of membrane permeation [31]. Passive diffusion is the most common route of drug absorption through membranes and tissues. Nevertheless, other routes of transport exist and the total percentage of the dose absorbed may be the result of a combination of several of these processes.

Primarily, the driving forces for the absorption of compounds through the gastrointestinal wall to reach systemic circulation are concentration differences, and thus, the rules of passive diffusion can be applied for both the transcellular penetration of lipophilic compounds and the paracellular diffusion of small polar compounds through and between gastrointestinal cells, respectively [30]. Other means of permeation that contribute to drug absorption are active transport by a transporter protein and endocytosis. Moreover, drugs can be effluxed by transporter proteins, such as P-gp or MRP2 (Figure 1.22).

Prior to absorption through the gastrointestinal cell walls, orally administered compounds need to dissolve in the aqueous contents of the gastrointestinal tract. This process depends on the surface area of the dissolving solid and the solubility of the drug at the surface of the dissolving solid [32]. Once the compound is dissolved, all further processes will take place in solution. Thus, solubility can be viewed as the first step to absorption. The solubility of the administered compound, in turn, depends on its physicochemical properties, for example, lipophilicity, ionization (pK_a), hydrogen bonding, molecular size, polarity, shape, and so on. Lipinski defined a widely accepted concept of druglikeness on the basis of cutoff values for key physicochemical properties known as the "rule of five" [33]. Accordingly, compounds are likely to show poor absorption when their molecular weight is >500 Da, their calculated octanol/water partition coefficient clog P is >5, the number of their H-bond donor functions is >5, and the number of their H-bond acceptor functions is >10. It has been suggested that drugs that fail to meet the "rule-of-five" criteria are unlikely to be absorbed and should be discontinued from development. Polar surface area (PSA) is another important parameter that is often taken into account for property-based design. It was deduced that orally active drugs that are passively transported by the transcellular route should not exceed a polar surface area of about 120 Å [34]. All these parameters can be calculated *in silico* by commercial programs that might be helpful in characterizing the physicochemical properties of a compound before it is even synthesized.

The incorporation of an ionizable moiety, such as a basic amine, into a template is a frequently employed means to improve a compound's aqueous solubility and hence absorption (Figure 1.23). Basic drugs will have increased solubility in the acidic

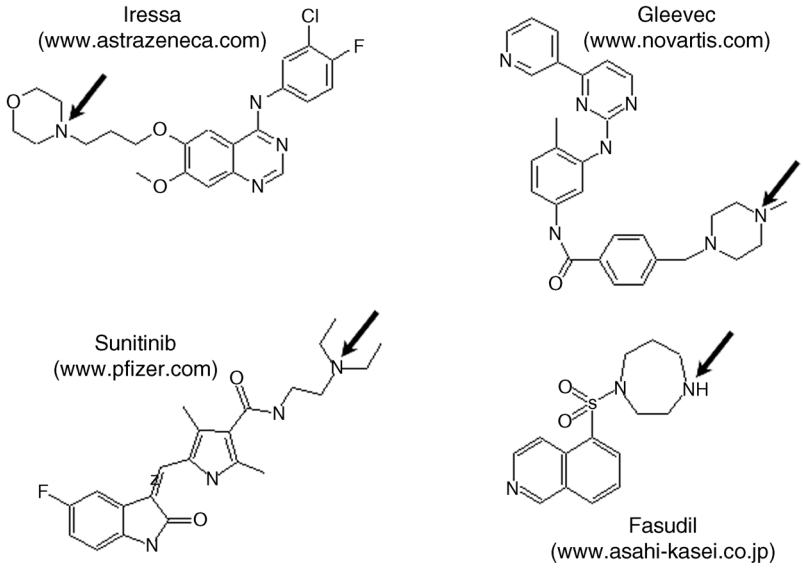

Figure 1.23 Structural formulas of approved ATP-competitive protein kinase inhibitors. Arrows point at secondary or tertiary amines that have been introduced as ionizable centers to improve aqueous solubility.

environment of the stomach where the dissolution of the compound usually takes place. In addition, if a drug has an ionizable center, then solubility can be improved by salt formation.

In contrast to the well-defined cutoff values of the rule of five, there is no generic guideline for the level of solubility sufficient to achieve oral absorption. Rather, estimates of the minimum solubility for oral absorption depend on the permeability of the compound and the required dose [35]. It has been shown that according to its permeability characteristics, the required solubility of a compound might vary between three orders of magnitude at various expected clinical potencies (Table 1.3).

To address drug absorption *in vitro*, scientists are, therefore, advised to embrace a whole set of models and methods that determine solubility, lipophilicity, ionization, permeability, and the interaction with transporters. Some of the most relevant experimental approaches and their predictive power for a potential absorption liability are reviewed below.

Table 1.3 Minimum acceptable solubility for low, medium, and high permeable compounds in μg/ml at a projected clinical dose to achieve oral absorption.

Projected clinical dose (mg/kg)	Low permeability	Medium permeability	High permeability
0.1	21	5	1
1.0	207	52	10
10	2100	520	100

Source: Adapted from Ref. [35].

1.4.2 Experimental Approaches to Drug Absorption

1.4.2.1 Measuring Solubility

As mentioned above, poor solubility is the key parameter to dissolution of compounds following oral administration that is likely to result in incomplete absorption. Experimentally, solubility can be determined under kinetic or thermodynamic conditions [36]. Thermodynamic solubility is the concentration of compound in a saturated solution when excess solid is present, and solution and solid are at equilibrium. Once this equilibrium has been established (24–72 h), the two phases are separated by filtration and/or centrifugation and the concentration of the compound in the dissolved phase is measured by HPLC–UV/Vis or HPLC–MS (shake flask method).

In contrast, kinetic solubility is the concentration of a compound in solution at the time when an induced precipitate first appears. Usually, kinetic solubility is measured from predissolved stocks (e.g., in DMSO) that are diluted in aqueous buffers followed by short read times in the low tens of minutes with or without filtration. The presence of a cosolvent has an impact on the apparent solubility of the compound. Since there is no crystal lattice to disrupt for compounds in DMSO solution, a compound's kinetic solubility is usually higher than the solubility value obtained from a thermodynamic experiment.

Measuring thermodynamic solubility by shake flask is thus more accurate than any apparent solubility determination by kinetic approaches. Moreover, the thermodynamic assay also provides additional information about the chemical stability and purity of the compound. However, as it is laborious and consumes larger amounts of compound, the throughput is normally far below kinetic solubility assay formats. Thus, although thermodynamic solubility measurements play only a minor role during the hit and lead generation phase of the drug discovery process, they are important during lead optimization, particularly when it comes to the selection of candidates for preclinical drug development. At this stage, the thermodynamic assay is a crucial test to conclude whether a compound has sufficient solubility to have the potential for oral activity.

In contrast, kinetic solubility assays can be viewed as early discovery formats that are most likely to predict the early drug metabolism or biology studies when the solubility assay conditions mimic the dosing schemes in early drug discovery experiments. A number of kinetic solubility assays have been developed most of which can be conducted under high-throughput conditions (Table 1.2).

1.4.2.2 Measuring Lipophilicity and Ionization

Lipophilicity is a key physicochemical parameter for the estimation of membrane permeability, distribution, and route of metabolic or renal clearance. Widely used parameters to measure lipophilicity are the partition coefficient (P) and the distribution coefficient (D):

$$P = [\mathrm{C}]_{\mathrm{o}}/[\mathrm{C}]_{\mathrm{w}}$$

$$D = \sum [\mathrm{C}]_{\mathrm{o}}/\sum [\mathrm{C}]_{\mathrm{w}}$$

where $[C]_o$ and $[C]_w$ are the concentrations of the compound in octanol (o) and in water (w), respectively.

The *P* value itself is a constant that defines the ratio of the concentration of the neutral form of the molecule between the two immiscible liquids, water and octanol. Substances with *P* values have elevated affinity for apolar solvents and are likely to show poor absorption if they exceed a *P* value of 10^5 (see the "rule of five"). *D* is the partition coefficient at a particular pH value and takes into account all the existing compound species in octanol or water/buffer. *D* is not constant and varies according to the protogenic nature of the molecule. It is normally convenient to use the logarithmic scale, log *P* and log *D*, for *P* and *D* values, respectively.

Log *D* at pH 7.4 is often quoted to give an indication of the lipophilicity of a drug at the pH of the blood. So, it has been suggested that log $D_{\mathrm{pH\ 7.4}}$ values between 1 and 3 are in the optimal range for orally active drugs evoking low metabolic liabilities. Above a log $D_{\mathrm{pH\ 7.4}}$ value of 3, metabolic liabilities tend to increase while poor solubility can become an issue. Clearly, log $D_{\mathrm{pH\ 7.4}}$ values above 5 should be avoided in order to minimize poor absorption, nonspecific binding, and high hepatic clearance while log $D_{\mathrm{pH\ 7.4}}$ values below 0 are associated with high renal clearance and poor permeability [37]. Lipophilicity can be increased by increasing molecular size and decreasing hydrogen-bonding capacity.

The pK_a is another important factor in drug design and development that is related to its effect on lipophilicity and solubility. This is because the majority of biologically active compounds comprise functional groups that can be ionized (see above). A high degree of ionization keeps drugs out of cells and decreases systemic toxicity. Thus, the pK_a has a high impact on both the partitioning behavior and the ligand interaction of the potential drug candidate. The pK_a is defined as the negative logarithm of the equilibrium ionization coefficient (K_a) of the neutral and charged forms of the compound.

$$\text{Equilibrium ionization constants for acids}: \quad K_a = [H^+][A^-]/[HA]$$
$$\text{Equilibrium ionization constants for bases}: \quad K_a = [H^+][B]/[HB]$$

Determination of the pK_a allows both to calculate the proportion of neutral and charged species at any pH and to define the basic or acidic properties of the compound. The pK_a itself is a constant and corresponds to the pH at which the concentrations of ionized and neutral forms are equal. It has been suggested that a pK_a in the range of 6–8 is advantageous for membrane penetration.

Since log *D* is a pK_a-dependent term for ionizable drugs, it is possible to calculate log *D* at any pH if log *P* and pK_a values are known. *In silico* tools exist for the calculation of log *P* and pK_a values that, although error prone for the prediction of log *D*, *per se* are useful in the design of log *D* assays in order to choose appropriate experimental conditions. *In vitro* methods for lipophilicity and ionization measurements are listed in Table 1.2.

1.4.2.3 **Measuring Permeability**

Since the oral route is often the preferred one for drug administration, an early estimate of the absorption potential across biological membranes is highly desirable.

A number of *in vitro* models for membrane permeability have been elaborated to date that allow the prediction of the diverse routes of drug absorption *in vivo* (for details see Ref. [38]).

The parallel artificial membrane assay (PAMPA) is a robust and reproducible assay for determining passive, transcellular compound permeation through an artificial lipid membrane made of lipophilic constituents [38]. In 1998, Kansy *et al.* [39] proposed a widely accepted model membrane permeation procedure consisting of filters coated with an alkane solution of lecithin with permeation rates being expressed as % flux values according to the equation:

$$\text{Flux}\,(\%) = [\text{C}]_{\text{test well}}/[\text{C}]_{\text{control well}} \times 100\%$$

where $[\text{C}]_{\text{test well}}$ is the concentration of the compound in the receiver well on the sample side and $[\text{C}]_{\text{control well}}$ is the concentration of the compound in the receiver well on the reference side.

PAMPA flux rates correlate well with passive human absorption values while obviously no prediction can be made for compounds that are actively transported or absorbed by the paracellular route [38].

This method can also be used to determine the effect of pH on compound permeability by adjusting the pH of the solutions used in the analysis. It is also possible to tailor the lipophilic constituents so that they mimic specific membranes such as the blood–brain barrier. Optimization of incubation time, lipid mixture, and lipid concentration can also enhance the assay's ability to predict compound permeability. Although, due to their lipophilic nature, poor flux values are rarely observed with ATP-competitive protein kinase inhibitors, the PAMPA model is nevertheless an indispensable tool for any holistic kinase inhibitor-directed ADME approach.

In addition, several cell-based assays have been developed for permeability screening capable of predicting oral absorption such as Caco-2 and Madin-Darby canine kidney cells (MDCK) [40]. The Caco-2 concept is of particular interest as it is associated with the kinetics of intestinal drug absorption, permeation enhancement, chemical moiety structure–permeability relationships, dissolution testing, and *in vitro/in vivo* correlation (Figure 1.24). In a typical Caco-2 experiment, a monolayer of cells is grown on a filter separating two stacked microwell plates. Test compounds can be introduced to either side of the cell layer and the rate of permeability through the cells is determined from A to B or from B to A according to the formula

$$P_{\text{app}}(\text{nm/s}) = (\text{d}Q/\text{d}t)/(A \times C_{\text{d0}})$$

where P_{app} is the apparent permeability coefficient and $\text{d}Q/\text{d}t$ is the rate of appearance of drug on the receiver side, C_{d0} is the initial drug concentration on the donor side, and A is the surface area of the filter membrane.

The assay requires that drug absorption rates be determined up to 21 days after Caco-2 cell seeding to allow monolayer formation and cell differentiation including the localization of active transporters to either side of the cell layer. Thus, the permeation observed in a fully differentiated Caco-2 monolayer is a composite of

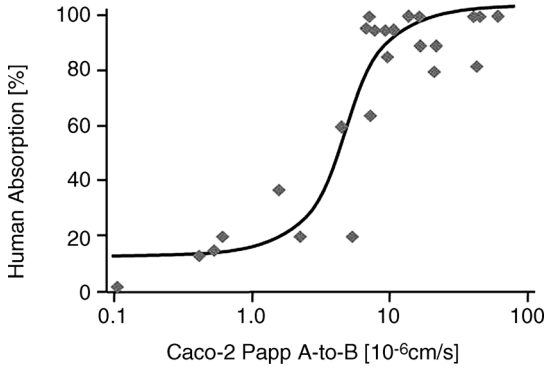

Figure 1.24 Correlation of drug transport rates with human absorption. Drug compounds representing active, passive, and efflux transporters were tested at ArQule, Inc. using the MultiScreen Caco-2 assay system. Each compound's permeability rate was plotted against their percent human absorption values [42].

multiple mechanisms of permeation such as passive transcellular diffusion, active transport through cells, paracelluar diffusion, and drug efflux. Furthermore, the presence of CYP450 and phase II conjugating enzymes enables the assessment of the metabolism of a drug during intestinal passage.

Many studies have shown that human oral drug absorption and Caco-2 permeability coefficient have a good sigmoidal relationship, suggesting that human absorption can be well predicted by this *in vitro* model [41].

1.4.2.4 **Transporter Assays Addressing P-gp Interaction**

The family of ATP binding cassette (ABC) transporters has been identified as a potentially limiting factor in drug absorption [43, 44]. All these proteins catalyze an ATP-dependent active transport of chemically unrelated compounds. Among the many ABC transporters that are expressed in the intestinal tissue, P-gp (MDR1) is perhaps the most studied. P-gp can actively transport a wide variety of chemically diverse compounds out of cells, but preferentially extrudes large hydrophobic, positively charged molecules. Besides intestinal cells, P-gp is present in hepatocytes, epithelial cells of the kidney, and endothelial cells of the blood–brain barrier that might affect not only the absorption but also the distribution and excretion of the drug administered. Due to the significance this transporter has for *in vivo* disposition and PK, identification of compounds that are P-gp substrates can aid optimization and selection of new drug candidates.

A variety of functional *in vitro* test systems have been used to classify compounds as P-gp substrates [45]. These assays either measure the translocation of a P-gp substrate or the substrate-triggered hydrolysis of ATP by P-gp. The interaction of a compound with P-gp can be determined indirectly by measuring the competition for P-gp-mediated transport between a reporter substrate and the compound. Alternatively, the interaction can be detected by directly measuring the translocation of the compound.

As mentioned above, Caco-2 cells provide a useful monolayer efflux method since they extensively express a variety of transport systems including P-gp that is especially advantageous in studies of the interplay between P-gp and other transporter proteins. The major drawback in using Caco-2 cells is that the transporter expression pattern changes with time. Thus, transfected cells are the experimental system of choice as they harbor a well-defined and more stable expression pattern. For instance, MDCKII-MDR1 cells, a transfected version of MDCKII cells that *per se* exhibit relatively low inherent expression of transporters, overexpress P-gp and are sensitive to determining P-gp efflux substrates [46].

The ATPase is one of the most widely used membrane-based assay systems to study the interaction of test compounds with P-gp [47]. Typically, membranes are prepared from recombinant baculovirus-infected insect cells, for example, Sf9 cells. The ATPase assay can determine whether or not a drug stimulates P-gp ATPase activity that would suggest that the drug is a substrate for P-gp transport. While ATP hydrolysis is required for drug transport, the ATPase assay does not directly measure drug transport (e.g., drugs can stimulate ATPase without being transported).

Like the ATPase assay, the whole cell-based calcein AM approach offers the advantage of higher throughput and generic readout in comparison to monolayer efflux assays [48]. Calcein AM is a nonfluorescent, cell membrane-permeable compound that, once inside the cell, can be hydrolyzed to a fluorescent dye that is retained inside the cell. This reaction is efficiently reduced in the presence of functional P-gp as calcein AM is extruded by P-gp. Thus, the intracellular accumulation of fluorescent calcein can be used as a measure of the extent of P-gp inhibition by test compounds. However, similar to ATPase method, the calcein AM assay is not designed to distinguish P-gp substrates from inhibitors.

1.4.3
Experimental Approaches to Drug Metabolism

1.4.3.1 Background and Concepts

Besides excretion of unchanged compounds, drug metabolism is one of the two major pathways for elimination of xenobiotics. Drug metabolism can affect a drug's behavior in many ways. For instance, first-pass metabolism of the compound may lead to a lower oral bioavailability while prodrugs need to be metabolized first to be active. Some metabolites of the administered drug might still be active, while some might be toxic. Furthermore, drug metabolism might have an impact on drug–drug interactions [49].

Traditionally, drug metabolism is divided into phase I and II processes. Compounds are typically oxidized, reduced, or hydrolyzed by phase I enzymes, while phase II metabolism encompasses all sorts of conjugative processes such as glucuronidation, acetylation, methylation, or addition of glutathione or sulfate (Table 1.4). The basic principle of drug metabolism is the conversion of xenobiotics into more hydrophilic inactive derivatives that are readily excreted. The liver is the primary site of drug metabolism although other organs (e.g., small intestine, kidney, lung, etc.) can play an important role.

Table 1.4 Division of metabolizing enzymes into phase I and phase II.

Process	Enzymes
Phase I: oxidation and reduction	Cytochromes P450 (CYP450s), flavin monooxygenase (FMO), peroxidases, amine oxidases, dehydrogenases, azo reductase
Phase I: hydrolysis	Proteases/peptidases, esterases, glucuronidases, sulfatases, phosphatases
Phase II: conjugation	Glucuronosyl transferases, glutathione transferases, sulfotransferases, methyl transferases, acetyl transferases, kinases

Phase I enzymes are normally oxidative and phase II conjugative.

The cytochrome P450 (CYP450) enzymes are involved in the metabolism of a wide range of drugs [50]. It has been observed that almost every drug is processed by CYP450 enzymes resulting in reduced bioavailability. CYP450s possess the unique ability to activate molecular oxygen to oxidizing species with the capacity to effect oxidation reactions extending from the hydroxylation at the unactivated carbon–hydrogen bond to the N- and S-oxidation of nitrogen and sulfur soft bases (Figure 1.25).

So far, 17 families of CYP450s representing about 50 isoforms have been characterized in the human genome, 3 of which, CYP2D6, CYP2C9, and CYP3A4, have been found to be involved in the metabolism of more than 80% of the pharmaceuticals in humans. Among other isoforms that are involved to a lesser extent CYP1A2 is especially interesting in the context of the optimization of kinase inhibitors as this CYP450 enzyme has a preference for flat molecules that is a common structural feature of ATP-competitive kinase inhibitor compounds (Figure 1.21).

Compounds that remain in the circulation after undergoing phase I metabolism often undergo phase II metabolism. In most of these reactions, a large polar group is added to the compound by transferase enzymes (see Table 1.4). Usually, this involves the interaction of the polar functional group of phase I metabolites, yet in some cases the parent compound might be a direct substrate for phase II metabolism if it provides an appropriate structural function.

One of the most important phase II conjugation reactions is that catalyzed by the UDP glucuronosyl transferase [51]. The glucuronidation reaction consists of the transfer of a glucuronosyl group from uridine 5′-diphosphoglucuronic acid (UDPGA) to substrate molecules that contain oxygen, nitrogen, sulfur, or carboxylic acid functional groups. The resulting glucuronide is ionic, more polar, frequently more water soluble, less toxic, and suitable for excretion in urine or bile.

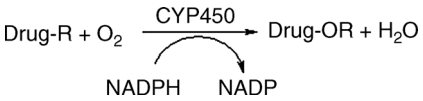

Figure 1.25 Overall scheme of a monooxidation reaction by CYP450s using NADPH as an electron-donating cofactor.

Ishikawa could show that after glucuronide conjugation of a drug, the adduct is recognized and transported into the bile by the hepatic transporter MRP2. Ishikawa proposed the term phase III metabolism for the canalicular export of drugs and drug metabolites from hepatocytes indicating the close connection between the oxidation and the conjugation steps of drug elimination [52, 53]. This concept has been expanded to other tissues where export pumps are present. All transporters involved in these mechanisms are members of the family of ATP binding cassette transporters (see Section 1.4.2.4), P-gp (MDR1, ABCB1), MRP2 (ABCC2), and BCRP (ABCG2) being the most prominent. All three transporters are present in the intestine and liver and therefore can reduce oral bioavailability by two mechanisms: direct inhibition of uptake out of the gut and rapid elimination of drugs and their metabolites via bile (Figure 1.26).

How efficiently xenobiotics are cleared by a given organ basically depends on three fundamental parameters: the flow of blood through the organ (Q), the intrinsic capability of the organ to clear the drug (CL_{int}), and the limitation on drug uptake into the clearing organ that in turn depends on the extent of binding of a drug to blood components (i.e., fraction unbound f_u in blood) [55].

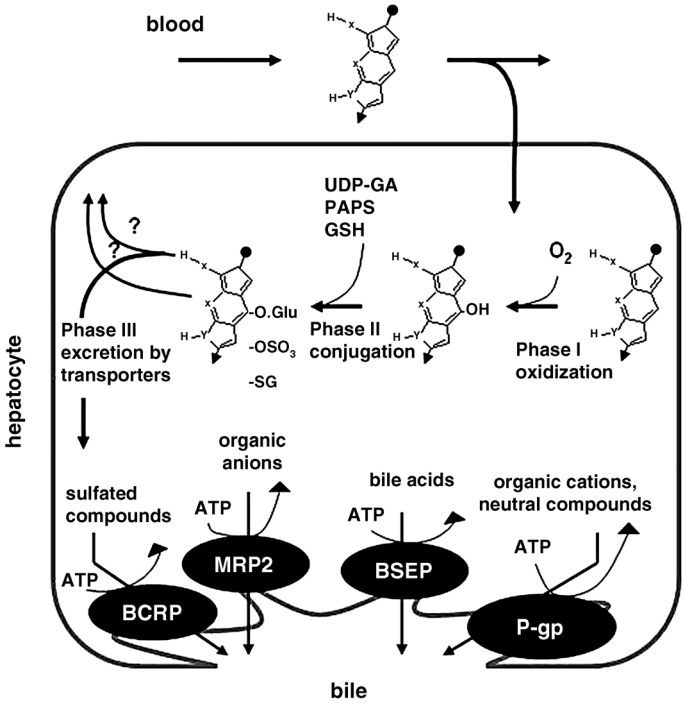

Figure 1.26 Phases of drug metabolism and biliary excretion in human hepatocytes (adapted from Ref. [54]). UDP-GA: uridine diphosphate glucuronic acid; PAPS: 3′-phosphoadenosin-5-phosphosulfate; GSH; glutathione.

Hepatic clearance (CL_H) is pharmacokinetically described by different mathematical models for the disposition of compounds in the liver such as well-stirred, parallel tube, and dispersion [56]. In their simplest forms, they all assume that the passage of a drug from blood in the liver is perfusion limited and that only unbound drug crosses the cell membrane and is available for metabolism.

For instance, under the assumption that the drug is mixed infinitely well inside the liver, the well-stirred model is applicable to the hepatic clearance (CL_H):

$$CL_H = Q_H \times f_{uB} \times CL_{uH,int}/(Q_H + f_{uB} \times CL_{uH,int})$$

where Q_H represents the hepatic blood flow, f_{uB} the fraction of drug unbound in blood, and $CL_{uH,int}$ the intrinsic metabolic clearance of the unbound drug in the liver.

Intrinsic metabolic clearance is a pure measure of enzyme activity toward a drug and is not influenced by other physiological determinants of liver clearance, that is, hepatic blood flow or drug binding within the blood matrix. There are several *in vitro* systems, such as primary hepatocytes, hepatic microsomes, or recombinantly expressed enzymes (see below) to measure the intrinsic metabolic clearance that is then used to estimate hepatic clearance in *in vitro–in vivo* extrapolations (Figure 1.27a).

In the absence of enzyme saturation, intrinsic metabolic clearance can be simply determined as the ratio of enzyme kinetic Michaelis–Menten parameters V_{max} and K_m (Equation 1.1). Alternatively, the *in vitro* intrinsic clearance rate can be derived from the rate of drug consumption related to the half-life of the drug in the *in vitro* system used (Equation 1.2):

1) $CL_{uH,int} = V_{max}/K_m$

2) $CL_{uH,int} = \ln 2/(in\ vitro\ t_{1/2})$

According to the *in vitro* system used, *in vitro* $CL_{uH,int}$ is expressed per million hepatocytes, per milligram microsomal protein basis, or per unit of recombinantly expressed enzyme. Using standard scaling factors, these *in vitro* values can be extrapolated to predict *in vivo* hepatic clearance on a per-kilogram body weight basis [57, 58].

Metabolic stability rates obtained from microsomal clearance experiments in conjunction with Caco-2 transport data have been used to predict the oral bioavailability of a diverse set of compounds. This model provides a good tool to estimate human oral bioavailability solely from *in vitro* ADME data especially if the oral bioavailability of the compound predominantly depends on permeability and metabolic clearance and not on other means of elimination, for example, renal or biliary excretion (Figure 1.27b).

1.4.3.2 **Measuring Metabolic Stability**

Although metabolic enzymes are present in many tissues, matrices prepared from ectomized liver are most often employed to investigate the metabolic stability of a test compound. Liver microsomes that can be obtained from various species provide a useful system to measure the rate of oxidative metabolism and formation of oxidative

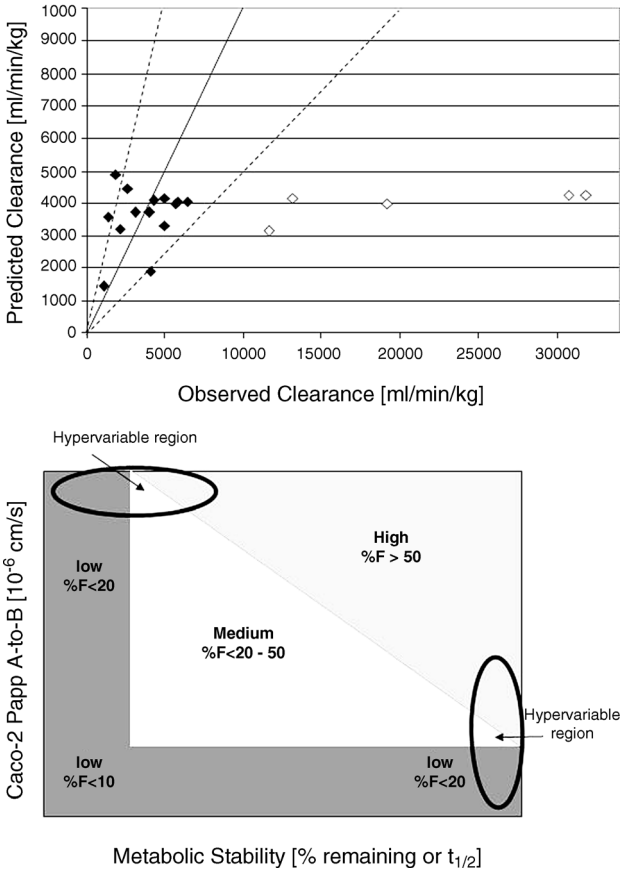

Figure 1.27 (a) Plot of mouse clearance values of diverse structural groups of kinase inhibitor compounds predicted from *in vitro* phase I intrinsic clearance data versus actual mouse clearance values. The prediction is based on the well-stirred model disregarding binding to plasma proteins or microsomal matrix. Most of the compounds fall inside the twofold error interval (dotted line). Outliers (indicated as white dots) are assumed to be cleared extrahepatically (Gimple *et al.*, unpublished data). (b) Graphical model for the prediction of oral bioavailability (*%F*) from Caco-2 Papp A to B values plotted against metabolic stability rates (adapted from Ref. [59]).

metabolites due to their high CYP450 activity [60]. However, phase II activity in liver microsomes is restricted to the conjugation of glucuronic acid by UDP glucuronosyl transferases (UGT). To study other phase II reactions, liver S9 fractions are a more appropriate system as they contain the microsomal and the cytosolic portion of liver cells. Although rather extensive and not readily available, freshly isolated hepatocytes represent the most comprehensive *in vitro* system for hepatic clearance as they encompass the full spectrum of hepatic phase I, phase II, and phase III enzymatic activities. Alternative tissues include cryopreserved hepatocytes and freshly isolated

liver slices. Finally, to exclusively study P450-mediated metabolism, higher throughput screening with human CYP450s is also available [61].

The preferred approach to metabolic stability is to incubate the compound in the matrix of choice against a control matrix containing no active CYP450 in a 96-well format. The remaining compound is detected by chromatographic analysis of the incubation medium followed by HPLC–MS/MS. Besides the determination of the clearance rate of the parental compound, this type of experiment leads to the direct identification of metabolites formed by oxidative, hydrolytic, or transferase reactions.

1.4.3.3 **Measuring CYP450 Inhibition**

Inhibition of CYP450s is an undesirable characteristic that may lead to drug–drug interactions [62]. *In vitro* experiments that are conducted to determine whether a drug inhibits a specific CYP450 enzyme involve incubation of the drug with probe substrates for CYP450 enzymes. Individually expressed CYP450 enzymes that can be obtained either from baculovirus-infected SF9 cells (supersomes) or from bacterial expression systems provide a convenient model to conduct P450 enzyme inhibition studies [63]. Fluorescence-based assays are available to determine CYP450 inhibition in a higher throughput. The inhibiting potential of compounds is usually tested at a wide range of concentrations on a series of probe substrates that are metabolized toward fluorescent metabolites and expressed as IC_{50} or K_i values. The assay format is in a 96-well plate that can be measured repeatedly in a fluorimeter to allow evaluation of time-dependent inhibition. In theory, significant CYP450 inhibition occurs when the concentration of the compound [I] at its site of action *in vivo* is comparable to or in excess of the K_i. $[I]/K_i$ ratios have been used to predict the likelihood of inhibitory drug–drug interactions *in vivo*; however, quantitative predictions of the magnitude of an *in vivo* interaction, based on *in vitro* data, are not yet possible.

Acknowledgment

We are grateful to Drs Séverine Dedier, Marc-Nicola Sommer, Edmund Hoppe, and Friedrich Kraetzer for numerous fruitful discussions.

References

1 Eason, I.H. and Stedman, E. (1936) The absolute activity of choline-esterase. *Proceedings of the Royal Society of London. Series B, Biological Sciences*, **121**, 142–164.

2 Strauss, O.H. and Goldstein, A. (1943) Zone behaviour of enzymes. *The Journal of General Physiology*, **26**, 559–585.

3 Cheng, Y.C. and Prusoff, W.H. (1973) Relationship between the inhibition constant (K1) and the concentration of inhibitor which causes 50 per cent inhibition (I50) of an enzymatic reaction. *Biochemical Pharmacology*, **22**, 3099–3108.

4 Michaelis, L. and Menten, M.I. (1913) Die Kinetik der Invertinwirkung. *Biochemische Zeitschrift*, **49**, 333–369.

5 Wu, G., Yuan, Y., and Hodge, N. (2003) Determining appropriate substrate

conversion for enzymatic assays in high throughput screening. *Journal of Biomolecular Screening*, **8**, 694–700.

6 Davies, S.P., Reddy, H., Caivano, M., and Cohen, P. (2000) Specificity and mechanism of action of some commonly used protein kinase inhibitors. *The Biochemical Journal*, **351**, 95–105.

7 Uehata, M., Ishizaki, T., Stoh, H., Ono, T., Kawahara, T., Morishita, T., Tamakawa, H., Yamagami, K., Inui, J., Maekawa, M., and Narumiya, S. (1997) Calcium sensitization of smooth muscle mediated by a Rho-associated protein kinase in hypertension. *Nature*, **389**, 990–994.

8 Huse, M. and Kuriyan, J. (2002) The conformational plasticity of protein kinases. *Cell*, **109**, 275–282.

9 Hubbard, S.R., Wei, L., Ellis, L., and Hendrickson, W.A. (1994) Crystal structure of the tyrosine kinase domain of the human insulin receptor. *Nature*, **372**, 746–754.

10 Schindler, T.C *et al.* (2000) Structural mechanism for STI-571 inhibition of Abelson tyrosine kinase. *Science*, **289**, 1938–1942.

11 Pargellis, C., Tong, L., Chruchill, L., Cirillo, P.F., Gilmore, T., Graham, A.G., Grob, P.M., Hickey, E.R., Moss, N., Pav, S., and Regan, J. (2002) Inhibition of p38 MAP kinase by utilizing a novel allosteric binding site. *Nature Structural Biology*, **9**, 268–272.

12 Mol, C.D., Fabbro, D., and Hosfield, D.J. (2004) Structural insights into the conformational selectivity of STI-571 and related kinase inhibitors. *Current Opinion in Drug Discovery & Development*, **7**, 639–648.

13 Copeland, R., Pompliano, D.L., and Meek, T.D. (2006) Drug–target residence time and its implications for lead optimization. *Nature Reviews. Drug Discovery*, **5**, 730–739.

14 Wood, E.R., Truesdale, A.T., McDonald, O.B., Yuan, D., Hassell, A., Dickerson, S.H., Ellis, B., Pennisi, C., Horne, E., Lackey, K., Alligood, K.J., Rusnak, D.W., Gilmer, T.M., and Shewchul, L. (2004) A unique structure for epidermal growth factor receptor bound to GW572016 (Lapatinib): relationship among protein conformation, inhibitor off-rate, and receptor activity in tumor cells. *Cancer Research*, **64**, 6652–6659.

15 Casper, D., Bukhtiyarova, M., and Springman, E.B. (2004) A Biacore biosensor method for detailed kinetic binding analysis of small molecule inhibitors of p38alpha mitogen-activated protein kinase. *Analytical Biochemistry*, **325**, 126–136.

16 Nordin, H., Jungnelius, M., Karlsson, R., and Karlsson, O.P. (2005) Kinetic studies of small molecule interactions with protein kinases using biosensor technology. *Analytical Biochemistry*, **340**, 359–368.

17 Rich, R.L. and Myszka, D.G. (2007) Higher-throughput, label-free- real time molecular interaction studies. *Analytical Biochemistry*, **361**, 1–6.

18 Kroe, R.R., Regan, J., Proto, A., Peet, G.W., Roy, T., Landro, L.D., Ruschetto, N.G., Pargellis, C.A., and Ingraham, R.H. (2003) Thermal denaturation: a method to rank slow binding, high-affinity P38alpha MAP kinase inhibitors. *Journal of Medicinal Chemistry*, **46**, 4669–4675.

19 Regan, J., Breitfelder, S., Cirillo, P., Gilmore, T., Graham, A.G., Hickey, E., Klaus, B., Madwed, J., Moriak, M., Moss, N., Pargellis, C., Pav, S., Proto, A., Swinamer, A., Tong, L., and Torcellini, C. (2002) Pyrazole urea-based inhibitors of p38 MAP kinase: from lead compound to clinical candidate. *Journal of Medicinal Chemistry*, **45** 2994–3008.

20 Regan, J., Pargellis, C.A., Cirillo, P.F., Gilmore, T., Hickey, E.R., Peet, G.W., Proto, A., Swinamer, A., and Moss, N. (2003) The kinetics of binding to p38 MAP kinase by analogues of BIRB 796. *Bioorganic & Medicinal Chemistry Letters*, **13**, 3101–3104.

21 Wilhelm, S.M., Carter, C., Tang, L., Wilkie, D., McNabola, A., Rong, H., Chen, C., Zhang, X., Vincent, P., McHugh, M., Cao, Y., Shujath, J., Gawlak, S., Eveleigh, D., Rowley, B., Liu, L., Adnane, L., Lynch, M., Auclair, D., Taylor, I., Gedrich, R., Vznesensky, A., Riedl, B., Post, L.E., Bollag, G., and Trail, P. (2004) BAY 43-9006 exhibits broad

spectrum oral antitumor activity and targets the RAF/MEK/ERK pathway and receptor tyrosine kinases involved in tumor progression and angiogenesis. *Cancer Research*, **64**, 7099–7109.

22 Wilhelm, S., Carter, C., Lynch, M., Lowinger, T., Dumas, J., Smith, R.A., Schwartz, B., Simanotov, R., and Kelley, S. (2006) Discovery and development of sorafenib: a multikinase inhibitor for treating cancer. *Nature Reviews. Drug Discovery*, **5**, 835–844.

23 Neumann, L., Ritscher, A., Mueller, G., and Hafenbradl, D. (2009) Fragment-based lead generation: identification of seed fragments by a highly efficient fragment screening technology. *Journal of Computer-Aided Molecular Design*, **23**, 501–511.

24 Liu, Y. and Gray, N. (2006) Rational design of inhibitors that bind to inactive kinase conformations. *Nature Chemical Biology*, **2**, 358–364.

25 (a) Backes, A.C., Zech, B., Felber, B., Klebl, B., and Mueller, G. (2008) Small-molecule inhibitors binding to protein kinases. Part I: exceptions from the traditional. *Expert Opinion on Drug Discovery*, **3** (12), 1371–1376; (b) Backes, A.C., Zech, B., Felber, B., Klebl, B., and Mueller, G. (2008) Small-molecule inhibitors binding to protein kinases. Part II: the novel pharmacophore approach of type II and type III inhibition. *Expert Opinion on Drug Discovery*, **3** (12), 1427–1449.

26 Kufereva, I. and Abagyan, R. (2008) Type-II kinase inhibitor docking, screening and profiling using modified structures of active kinase states. *Journal of Medicinal Chemistry*, **51** (24), 7921–7932.

27 Kola, I. and Landis, J. (2004) Can the pharmaceutical industry reduce attrition rates? *Nature Reviews. Drug Discovery*, **3** (8), 711–715.

28 Balani, S.K., Miwa, G.T., Gan, L.S., Wu, J.T., and Lee, F.W. (2005) Strategy of utilizing *in vitro* and *in vivo* ADME tools for lead optimization and drug candidate selection. *Current Topics in Medicinal Chemistry*, **5** (11), 1033–1038.

29 Wishart, D.S. (2007) Improving early drug discovery through ADME modelling: an overview. *Drugs in R&D*, **8** (6), 349–362, Review.

30 Weiss, T.F. (1996) *Cellular Biophysics: Transport*, Vol. **1**, The MIT Press, Cambridge, MA.

31 Van de Waterbeemd, H. (2000) in *Oral Drug Absorption: Prediction and Assessment* (eds J.B. Dressman and H. Lenneräs), Dekker, New York, pp. 31–49.

32 Horter, D. and Dressman, J.B. (2001) Influence of physicochemical properties on dissolution of drugs in the gastrointestinal tract. *Advanced Drug Delivery Reviews*, **46** (1–3), 75–87.

33 Lipinski, C.A. (1997) Experimental and computational approaches to estimate solubility and permeability in drug discovery and development settings. *Advanced Drug Delivery Reviews*, **23** (1–3), 3–25.

34 Clark, D.E. (1999) Rapid calculation of polar molecular surface area and its application to the prediction of transport phenomena. 1. Prediction of intestinal absorption. *Journal of Pharmaceutical Sciences*, **88**, 807–814.

35 Lipinski, C.A. (2000) Drug-like properties and the cause of poor solubility and poor permeability. *Journal of Pharmacological and Toxicological Methods*, **44**, 235–249.

36 Bhattachar, S.N., Deschenes, L.A., and Wesley, J.A. (2006) Solubility: it's not just for physical chemists. *Drug Discovery Today*, **11** (21–22), 1012–1018.

37 Shalaeva, M. (2002) New Technologies to Increase Drug Candidate Survivability Conference, Philadelphia, PA, March 2002.

38 (2006) *Drug Bioavailability*, Wiley-VCH Verlag GmbH, Weinheim.

39 Kansy, M., Senner, F., and Gebernator, K. (1998) Physicochemical high throughput screening: parallel artificial membrane permeability assay in the description of passive absorption processes. *Journal of Medicinal Chemistry*, **41**, 1007–1010.

40 Press, B. and Di Grandi, D. (2008) Permeability for intestinal absorption: Caco-2 assay and related issues. *Current Drug Metabolism*, **9** (9), 893–900.

41 Artursson, P., Palm, K., and Luthman, K. (2001) Caco-2 monolayers in experimental and theoretical predictions of drug

transport. *Advanced Drug Delivery Reviews*, **46** (1–3), 27–43.

42 Yu, H.C *et al.* (2002) Validation of 96-well insert plates in the Caco-2 permeability screening assay. Poster presented at the AAPS Annual Meeting and Exposition, Toronto, Canada.

43 Schinkel, A.H. and Jonker, J.W. (2003) Mammalian drug efflux transporters of the ATP binding cassette (ABC) family: an overview. *Advanced Drug Delivery Reviews*, **55** (1), 3–29.

44 Colabufo, N.A., Berardi, F., Contino, M., Niso, M., and Perrone, R. (2009) ABC pumps and their role in active drug transport. *Current Topics in Medicinal Chemistry*, **9** (2), 119–129.

45 Glavinas, H., Krajcsi, P., Cserepes, J., and Sarkadi, B. (2004) The role of ABC transporters in drug resistance, metabolism and toxicity. *Current Drug Delivery*, **1** (1), 27–42.

46 Volpe, D.A. (2008) Variability in Caco-2 and MDCK cell-based intestinal permeability assays. *Journal of Pharmaceutical Sciences*, **97** (2), 712–725.

47 Sharom, F.J. (2006) Shedding light on drug transport: structure and function of the P-glycoprotein multidrug transporter (ABCB1). *Biochemistry and Cell Biology*, **84** (6), 979–992.

48 Szakács, G., Jakab, K., Antal, F., and Sarkadi, B. (1998) Diagnostics of multidrug resistance in cancer. *Pathology Oncology Research*, **4** (4), 251–257.

49 Korfmacher, W.A. (2009) Advances in the integration of drug metabolism into the lead optimization paradigm. *Mini-Reviews in Medicinal Chemistry*, **9** (6), 703–716.

50 Venkatakrishnan, K., Von Moltke, L.L., and Greenblatt, D.J. (2001) Human drug metabolism and the cytochromes P450: application and relevance of *in vitro* models. *Journal of Clinical Pharmacology*, **41** (11), 1149–1179.

51 Testa, B. and Krämer, S.D. (2008) The biochemistry of drug metabolism: an introduction. Part 4. Reactions of conjugation and their enzymes. *Chemistry & Biodiversity*, **5** (11), 2171–2336.

52 Ishikawa, T. (1992) The ATP-dependent glutathione S-conjugate export pump. *Trends in Biochemical Sciences*, **7** (11) 463–468.

53 Chandra, P. and Brouwer, K.L. (2004) The complexities of hepatic drug transport: current knowledge and emerging concepts. *Pharmaceutical Research*, **21** (5), 719–735.

54 Ito, K., Suzuki, H., Horie, T., and Sugiyama, Y. (2005) Apical/basolateral surface expression of drug transporters and its role in vectorial drug transport. *Pharmaceutical Research*, **22** (10), 1559–1577.

55 Wilkinson, G.R. and Shand, D.G. (1975) A physiological approach to hepatic drug clearance. *Clinical Pharmacology and Therapeutics*, **18**, 377–390.

56 Iwatsubo, T., Hirota, N., Ooie, T., Suzuki, H., Shimada, N., Chiba, K., Ishizaki, T., Green, C.E., Tyson, C.A., and Sugiyama, Y. (1997) Prediction of *in vivo* drug metabolism in the human liver from *in vitro* metabolism data. *Pharmacology & Therapeutics*, **73**, 147.

57 McGinnity, D.F., Soars, M.G., Urbanowicz, R.A., and Riley, R.J. (2004) Evaluation of fresh and cryopreserved hepatocytes as *in vitro* drug metabolism tools for the prediction of metabolic clearance. *Drug Metabolism and Disposition: The Biological Fate of Chemicals*, **32** (11), 1247–1253.

58 Obach, R.S. (2001) The prediction of human clearance from hepatic microsomal metabolism data. *Current Opinion in Drug Discovery & Development*, **4** (1), 36–44.

59 Mandagere, A., Thompson, T.N., and Hwang, K.K. (2002) Graphical model for estimating oral bioavailability of drugs in humans and other species from their Caco-2 permeability and *in vitro* liver enzyme metabolic stability rates. *Journal of Medicinal Chemistry*, **45** (2), 304–311.

60 Rane, A., Wilkinson, G.R., and Shand, D.G. (1977) Prediction of hepatic extraction ratio from *in vitro* measurement of intrinsic clearance. *The Journal of Pharmacology and Experimental Therapeutics*, **200** (2), 420–424.

61 Crespi, C.L. (1999) Higher through put screening with human cytochrome

P450s. *Current Opinion in Drug Discovery & Development*, **2**, 15–19.

62 Hutzler, M., Messing, D.M., and Wienkers, L.C. (2005) Predicting drug–drug interactions in drug discovery: where are we now and where are we going? *Current Opinion in Drug Discovery & Development*, **8** (1), 51–58.

63 Crespi, C.L. and Penman, B.W. (1997) Use of cDNA-expressed human cytochrome P450 enzymes to study potential drug–drug interactions. *Advances in Pharmacology*, **43**, 171–188.

64 Kabasakalian, P., Britt, E., and Yudis, M.D. (1966) Solubility of some steroids in water. *Journal of Pharmaceutical Sciences*, **55** (6), 642.

65 Bevan, C.D. and Lloyd, R.S. (2000) A high-throughput screening method for the determination of aqueous drug solubility using laser nephelometry in microtiter plates. *Analytical Chemistry*, **72** (8), 1781–1787.

66 Avdeef, A. (2001) Physicochemical profiling (solubility, permeability and charge state). *Current Topics in Medicinal Chemistry*, **1** (4), 277–351.

67 Avdeef, A., Box, K.J., Comer, J.E., Hibbert, C., and Tam, K.Y. (1998) pH-metric log *P* 10. Determination of liposomal membrane–water partition coefficients of ionizable drugs. *Pharmaceutical Research*, **15** (2), 209–215.

68 Valko, K., My Du, C., Bevan, C., Reynolds, D.P., and Abraham, M.H. (2001) Rapid method for the estimation of octanol/water partition coefficient (log *P*(oct)) from gradient RP-HPLC retention and a hydrogen bond acidity term (zetaalpha(2)(H)). *Current Medicinal Chemistry*, **8** (9), 1137–1146.

69 Avdeef, A. (1993) pH-metric log *P*. II. Refinement of partition coefficients and ionization constants of multiprotic substances. *Journal of Pharmaceutical Sciences*, **82** (2), 183–190.

70 Polli, J.W., Wring, S.A., and Humphreys, J.E. (2001) Rational use of *in vitro* P-glycoprotein assays in drug discovery. *The Journal of Pharmacology and Experimental Therapeutics*, **299**, 620–628.